CHAPTER 5

Therapeutic expression of hairpins targeting Apolipoprotein B100 induces differential changes in murine liver

Piotr Maczuga[1,2], Joanne Verheij[3], Chris van der Loos[3], Richard van Logtenstein[1], Gerrit Hooijer[3], Florie Borel[1,4], Jacek Lubelski[1], Annemart Koornneef[1], Bas Blits[1], Sander van Deventer[2], Harald Petry[1] and Pavlina Konstantinova[1]

[1]Department of Research & Development, uniQure Biopharma B.V., Amsterdam, the Netherlands; [2]Department of Gastroenterology and Hepatology, Leiden University Medical Center, Leiden, the Netherlands; [3] Department of Pathology, Academic Medical Center, Amsterdam, the Netherlands; [4] Department of Gastroenterology and Hepatology, Academic Medical Center, Amsterdam, the Netherlands

Submitted to Gene Therapy

Abstract

Constitutive expression of short-hairpin RNAs (shRNAs) may cause cellular toxicity *in vivo* and using microRNA (miRNA) scaffolds can circumvent this problem. Here we show that embedding siRNA sequences targeting Apolipoprotein B100 (ApoB) in shRNA (shApoB) or miRNA (miApoB) scaffolds resulted in differential processing and efficacy, leading to changes in liver morphology, cellular miRNA and gene expression. Adeno-associated virus (AAV)-shApoB- or AAV-miApoB-mediated ApoB knockdown induced differential expression of 37 cellular miRNAs and significant deregulation of 106 and 266 genes, respectively. Overall, our data indicate that therapeutic expression of shApoB and miApoB results in alterations of different lipid metabolism genes despite the same phenotypic effect of plasma cholesterol reduction. Surprisingly, only in AAV-shApoB-injected animals, genes involved in immune system activation or cell growth and death were affected, which was represented with increased hepatocyte proliferation in this group. Subsequently, in AAV-miApoB-injected animals, changes of genes involved in oxidoreductase activity, oxidative phosphorylation and nucleic bases biosynthetic processes were observed indicating that shApoB and miApoB have a distinct side effect profile. Deregulation of cellular miRNA and liver transcriptome may have serious consequences for future RNAi therapeutics as it may result in cytotoxicity and loss of gene silencing.

Introduction

RNAi is an evolutionary conserved sequence-specific post-transcriptional gene silencing mechanism in eukaryotes that results in the degradation of mRNA and subsequently in decrease of protein synthesis [1]. Therapeutic RNAi can be induced by delivering synthetic small interfering RNAs (siRNAs) or by intracellular expression of short hairpin RNAs (shRNAs) and artificial microRNAs (miRNAs) that target a disease-causing gene [2,3,4]. shRNAs and miRNAs are typically expressed in the cell from pol III or pol II promoters, respectively and are processed by the RNAi machinery, rendering a mature siRNA, which interacts with the cytosolic multiprotein RNA-induced silencing complex (RISC). The RISC-incorporated siRNA binds to the complementary mRNA sequence and mediates its sequence-specific degradation or translational repression [5,6].

Because RNAi can interfere with normal functioning of the cells, the safety of RNAi therapeutics is a major issue. Non-specific effects resulting from the RNAi induction appear to have several main causes: oversaturation of the RNAi pathway, aspecific activation of the immune response and off-target effects due to miRNA-like binding [7-12]. These side effects are often associated with severe toxicity, which can be even fatal. High expression levels of therapeutic shRNA can saturate the endogenous RNAi machinery and in consequence lead to deregulation of the entire miRNA network. For example, mice injected with AAV expressing shRNAs against different targets, developed liver failure irrespective of hairpin length, sequence, and target [10]. Toxicity could be circumvented by using lower vector doses, but this approach in some cases resulted in loss of RNAi silencing efficacy and therapeutic effect [13]. Alternatively, toxicity resulting from shRNA overexpression can be resolved by embedding the siRNA sequence into an artificial miRNA scaffold and expressing it from weaker pol II promoters [4,14,15]. By using miRNA scaffolds disruption of the endogenous RNAi pathway is avoided and shRNA-induced cell death can be prevented. However, in some cases miRNA were found to be less potent compared to shRNA [13].

A second source of toxicity is immune system activation. Characteristically, the interferon (IFN) response to foreign double-stranded RNAs (dsRNAs) is either mediated by phosphorylation of the dsRNA-dependent protein kinase R (PKR) leading to a global inhibition of protein synthesis [16] or via Toll-like receptor (TLR) activation [17]. Recent studies showed that RNAi therapeutics, in particular siRNAs can be potent inducers of IFN and inflammatory cytokines both *in vivo* and *in vitro* [9,11]. Administration of siRNA for treatment of neovascular age-related macular degeneration (AMD) has been reported to induce retinal degeneration via non-specific activation of immune response, which was independent of siRNA or target sequence [18]. Although intracellulary expressed shRNAs are less prone to IFN activation because they can evade activation of TLR, several reports indicated immune reactions against vector delivered shRNA. For example, adenoviral delivery of shRNA targeting Fatty acid

binding protein 5 (Fabp5) activated IFN response in liver [19] and lentiviral vector delivery of shRNA targeting Cyclophilin resulted in IFN activation *in vitro* [20].

Another source of RNAi toxicity is aspecific deregulation of gene expression, when non-targeted transcripts are down-regulated based on sequence complimentarily to the shRNA or miRNA "seed" sequence [12,21]. Because of the complexity of shRNA and miRNA processing and RISC loading, these unanticipated interactions are difficult to predict and evaluate. Off-targeting can be minimized by adopting a stringent design filter both for sense and antisense strands of the RNAi efector molecules. This approach has been validated for siRNA targeting Huntingtin, where off-targeting effect was significantly minimized by avoiding complementarity of siRNA "seed" to 3'UTR, while a high silencing potential was maintained [22]. Additionally significant reduction of off-target effects can be achieved by reducing the dose of siRNA or by chemical modification which impairs siRNA binding to possible off-targets [23].

Previously we have identified differences in processing and efficacy of shRNA and artificial miRNA targeting Apolipoprotein B100 (ApoB) that resulted in differences in long-term gene silencing *in vivo* when delivered with self-complementary adeno-associated virus serotype 8 (AAV) [24]. In the present study we investigated the effect of AAV-shApoB and AAV-miApoB expression on liver morphology, cell proliferation, cellular miRNA and transcriptome changes. Using both approaches, a strong decrease of plasma cholesterol was observed *in vivo* without signs of serious side-effects. Although biochemical analysis showed no acute toxicity, the AAV-shApoB and AAV-miApoB induced differential changes in liver histology, miRNA and transcriptome profiles. Hepatic steatosis, which is known side-effect of ApoB inhibition, was observed with both molecules. However in AAV-shApoB-injected animals increased proliferation of hepatocytes was observed as compared to AAV-miApoB and only in AAV-shApoB-injected animals, genes involved in immune response, cell growth and death were found to be affected.

Results

Knockdown efficacy of AAV-delivered shApoB and miApoB in murine liver

We have previously reported that identical AAV-delivered siApoB sequences in shApoB and miApoB scaffolds (Fig. 1a) are differently processed and have a dissimilar knockdown efficacy *in vivo* [24]. miApoB had a better long-term efficacy and resulted in a more sustained reduction of plasma ApoB and cholesterol in mice. The reduction of therapeutic efficacy was associated with a loss of virally-delivered DNA, but no obvious signs of RNAi toxicity were observed. To directly compare the safety profile of shApoB and miApoB, male C57Bl/6 mice were injected with 1×10^{11} gc AAV per animal encoding shApoB, miApoB, shScr and miScr. All viruses co-expressed enhanced green fluorescent protein (eGFP) for monitoring of liver transduction efficacy and eGFP only

expressing virus (AAV-GFP) was used as an additional control. Mice were sacrificed at week 8 post injection (p.i.) and liver samples were collected for histological and molecular analysis. According to eGFP fluorescence intensity liver transduction efficacy was ~50% (Fig. 1b), and at week 8 ApoB mRNA was reduced by 80% in AAV-shApoB and 87% in AAV-miApoB-injected animals (Fig. 1c). This resulted in 60% and 70% inhibition of plasma cholesterol, respectively (Fig. 1d). Quantification of siApoB molecules expressed from both shApoB and miApoB showed that the knockdown effect correlated to siRNA expression in the liver and AAV-miApoB transduction resulted in significantly less siApoB molecules (Fig. 1e).

It has been reported that expression of shRNA may lead to severe liver toxicity symptoms that is associated with an increase of plasma levels of the transaminases alanine aminotransferase (ALT) and aspartate aminotransferase (AST). Mice injected with AAV-miScr eshowed a mild increase in ALT levels at weeks 4 and 6 p.i., which returned to baseline at week 8 p.i. (Fig. 1f). AAV-miApoB injection gave rise to a two- to three- fold increase in ALT at week 4 p.i. and AST at week 6 p.i. (Fig. 1f). In contrast, no significant increase in liver transaminases for the AAV-shScr, AAV-shApoB and AAV-GFP-injected animals was observed (Fig. 1f). Mouse body weight did not change in any groups and none of the animals displayed any signs of illness or discomfort (data not shown).

Expression of shApoB increases hepatocyte proliferation *in vivo*

A histological analysis was performed to evaluate the effect of stable expression of shApoB and miApoB on liver morphology. ApoB suppression results in decreased cholesterol levels due to impairment of VLDL-C and LDL-C assembly [25] but can also lead to hepatic triglyceride accumulation [26-28]. Triglycerides are normally incorporated into VLDL-C and hepatic accumulation of these lipids can potentially cause steatosis. To investigate the effect of ApoB knockdown on liver morphology, a scoring system was developed and was used to score hematoxylin and eosin (H&E) liver sections (Table S1). Histological analysis revealed no gross changes in liver morphology and no signs of lobular or portal inflammation or parenchymal necrosis were detected in any group (Fig. 2a). However in AAV-shApoB- and AAV-miApoB-injected animals, microvesicular steatosis affecting more than 67% of the liver tissue was apparent (Table 1 and Fig. 2a). In addition, an increase in the hepatocellular mitosis rate was found in AAV-shApoB-injected animals (Table 1). To confirm the scoring results and assess the effect of ApoB knockdown on hepatic lipid accumulation, Oil red O staining was performed on liver sections. Increased accumulation of hepatic lipid content in AAV-shApoB- and AAV-miApoB-injected animals compared to control groups was detected (Fig. 2b).

Previously we have demonstrated that the silencing effect of AAV-shApoB and AAV-miApoB waned over time and this was associated with a loss of virally delivered DNA [24]. We hypothesized that the loss of the (non-integrated) silencing construct

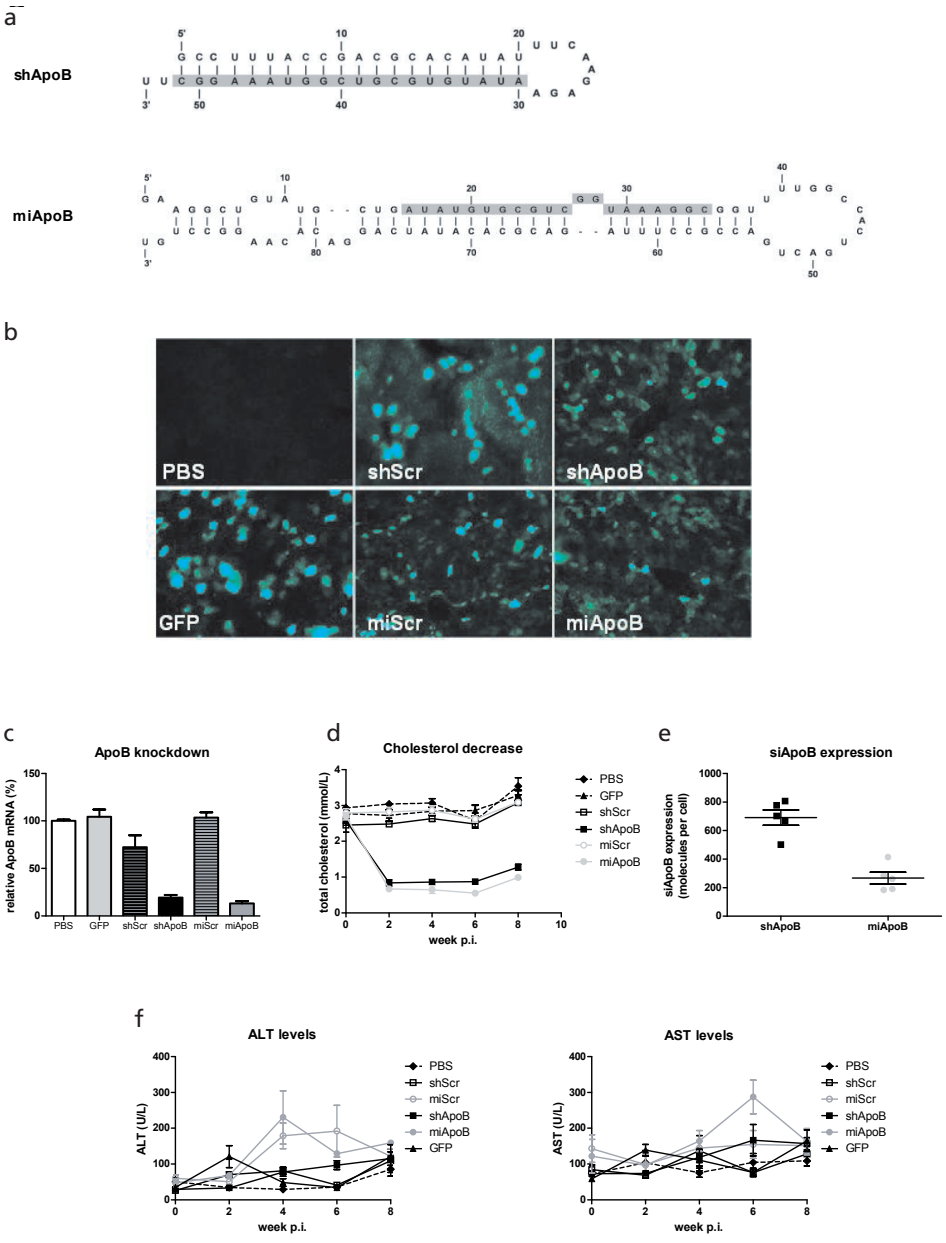

Figure 1. Structure, knockdown efficacy of AAV-shApoB and AAV-miApoB, siApoB expression and ALT/AST levels *in vivo*. Male C57BL/6 mice were intravenously injected with $1x10^{11}$ gc AAV-shApoB, AAV-miApoB, AAV-shScr, AAV-miScr, AAV-GFP or PBS. Plasma was collected every two weeks p.i., animals were sacrificed at 8 weeks p.i. and liver samples were collected for analysis (a) Predicted stem-loop structure for shApoB and miApoB with the guide strand shown in grey. (b) Representative image of GFP fluorescence in snap-frozen livers, transduced with 10^{11} gc of the indicated viruses. Photos were taken using the same exposure and magnification settings. (c) Relative ApoB mRNA expression in murine liver 8 weeks p.i. Total RNA was isolated from snap-frozen liver ►

► tissues and qRT-PCR was performed using ApoB- and actin-specific primers. ApoB mRNA levels were calculated relative to actin mRNA. ApoB mRNA levels in the PBS group was set at 100 %. Data are represented as mean values ±SE (d) Total cholesterol levels in plasma collected from fasted mice over the course of 8 weeks p.i. Cholesterol levels were analyzed on the automated clinical chemistry analyzer Modular Analytics P800. (e) siRNA expression in murine liver 8 weeks p.i. Total RNA was isolated from snap-frozen tissues and siApoB-specific small RNA TaqMan was performed. siApoB copy number was calculated using a siApoB synthetic RNA oligo standard line. Data are represented as mean values ±SE. (f) Plasma ALT (left panel) and AST (right panel) levels at 0, 2, 4, 6 and 8 weeks p.i. Transaminases were analyzed on the automated clinical chemistry analyzer Modular Analytics P800. Data are represented as mean ±SE, treatment groups are n = 5.

could have resulted from either cell division or cell death. Histological scoring showed an increase of proliferating hepatocytes in AAV-shApoB-injected animals, but no increase of apoptotic cells was observed in any of the groups (Table 1). To confirm these histological findings, we first examined whether AAV-shApoB or AAV-miApoB administration enhances the proliferative state of the liver cells. Two major types of cells populate the liver lobes: parenchymal referred as hepatocytes and non-parenchymal cells-sinusoidal cells. To distinguish between proliferating hepatocytes and sinusoidal cells slides were simultaneously stained with antibodies against cytokeratine 18 (CK18), which is a marker for hepatocytes, anti-CD31, a known marker for sinusoidal cells, and the Ki67 antigen, a known marker for cell proliferation (Fig. 2c). Surprisingly the number of proliferating hepatocytes was increased ~2 fold in AAV-shApoB animals compared to AAV-miApoB and control groups (Fig. 2d). When livers were stained for cleaved caspase 3, no increased apoptosis was detected in any of the animal groups (Fig. 2e).

Table 1. Histological scoring of H&E liver sections. Mice were intravenously injected with $1x10^{11}$ gc AAV-shApoB or AAV-miApoB, or their respective controls AAV-shScr, AAV-miScr, AAV-GFP and PBS. Animals were sacrificed at 8 weeks p.i. and liver samples were collected for analysis Paraffin embedded liver sections were stained with H&E and blind histological scoring was performed. Detailed information about the the scoring system used can be found in Table S1. *p<0,05 One-way ANOVA with Bonferroni post test against PBS.

	AVERAGE SCORE					
ITEM	shScr	shApoB	miScr	miApoB	shGFP	PBS
Macrovesicular steatosis	0	0	0	0	0	0
Microvesicular steatosis	1	3*	0	3*	0	0
Ballooning	0	0	0	0	0	0
Lobular inflammation	1	1	1	1	1	1
Portal inflammation	1	0	0	1	0	1
Sinusoidal dilatation	0	0	0	0	0	0
Parenchymal necrosis	0	0	0	0	0	0
Hepatocellular mitosis	1	2*	0	0	0	0
Councilman bodies	0	0	1	1	1	1

shApoB and miApoB expression induces differential cellular miRNA expression

Overexpression of therapeutic shRNAs and miRNAs can modify the processing of cellular miRNA transcripts since they share the same processing pathway and nuclear export machinery. We investigated whether high expression of shApoB and miApoB competes with the intracellular processing of miRNAs *in vitro* and *in vivo*. Next generation sequencing (NGS) of small RNAs was performed on HEK293T cells transfected with shApoB- or miApoB-expression constructs. Expression of endogenous miRNAs was normalized to mir-92 and expressed as number of reads per million (rpm). All conserved mammalian miRNAs with more than a 2-fold change between miApoB and shApoB were included in the statistical comparison. Kal's test (Z-test) with Bonferroni correction was used to compare the expression values of the cellular miRNAs in the miApoB- versus shApoB-transfected cells. A total of 37 cellular miRNAs, were found to be differentially expressed (Fig. 3a). A complete list of the differentially expressed miRNAs in the miApoB- versus shApoB-transfected cells can be found in Supplementary Table 2.

To determine whether shApoB and miApoB expression *in vivo* also results in different cellular miRNA profiles, endogenous levels of 7 miRNAs that are expressed in liver were measured *in vivo* 8 wk p.i. for all animal groups (Fig. 3b). The levels of the liver-specific mir-122 and the broadly expressed miRNAs let-7a, let-7e, mir-26a and mir-221 were not significantly changed in any of the groups expressing shApoB or miApoB. Expression levels for all miRNAs tested were in the range of 80% to 200% of the levels measured in PBS-treated animals. Mir-133a and mir-199a expression was 2-3 fold upregulated in AAV-miApoB-injected animals compared to PBS-injected animals. Importantly, mir-133a expression was significantly different in AAV-miApoB group compared to AAV-shApoB.

Figure 2. Effect of AAV-delivered shApoB and miApoB on liver morphology, proliferation and hepatic fat accumulation. Mice were intravenously injected with $1x10^{11}$ gc AAV-shApoB or AAV-miApoB, or their respective controls AAV-shScr, AAV-miScr, AAV-GFP and PBS. Animals were sacrificed at 8 weeks p.i. and liver samples were collected for analysis. (a) Representative image of H&E liver morphology staining. Paraffin embedded liver sections were stained with eosin for cytoplasm visualization, and nuclei were counterstained with hematoxylin solution. (b) Representative image of hepatic lipid accumulation. Frozen liver sections were stained with Oil Red O for lipids, and nuclei were counterstained with hematoxylin solution. (c) Representative image of liver proliferation. Paraffin embedded liver sections were simultaneously stained in red for hepatocytes (Rabbit anti-mouse CK18), in brown for sinusoidal cells (rabbit anti-mouse CD31) and in blue for antigen Ki67 (Rabbit ant-mouse Ki67). A nuclei counterstaining with hematoxylin was performed. (d) Representative image of liver apoptosis. Paraffin embedded liver sections were stained in blue for cleaved-Caspase 3 (Rabbit anti-mouse). Nuclei counterstaining with hematoxylin was performed. (e) Quantification of proliferating hepatocytes staining described in c). Spectral decomposition was done using inForm software v1.4 and the amount of proliferating hepatocytes (CK18+, Ki67+) was calculated for each animal in 5 different visual fields. Data are represented as mean values of 5 animals ±SE. ***$p < 0.001$ One-way ANOVA with Bonferroni post test against PBS. Bar = 5 µm ►

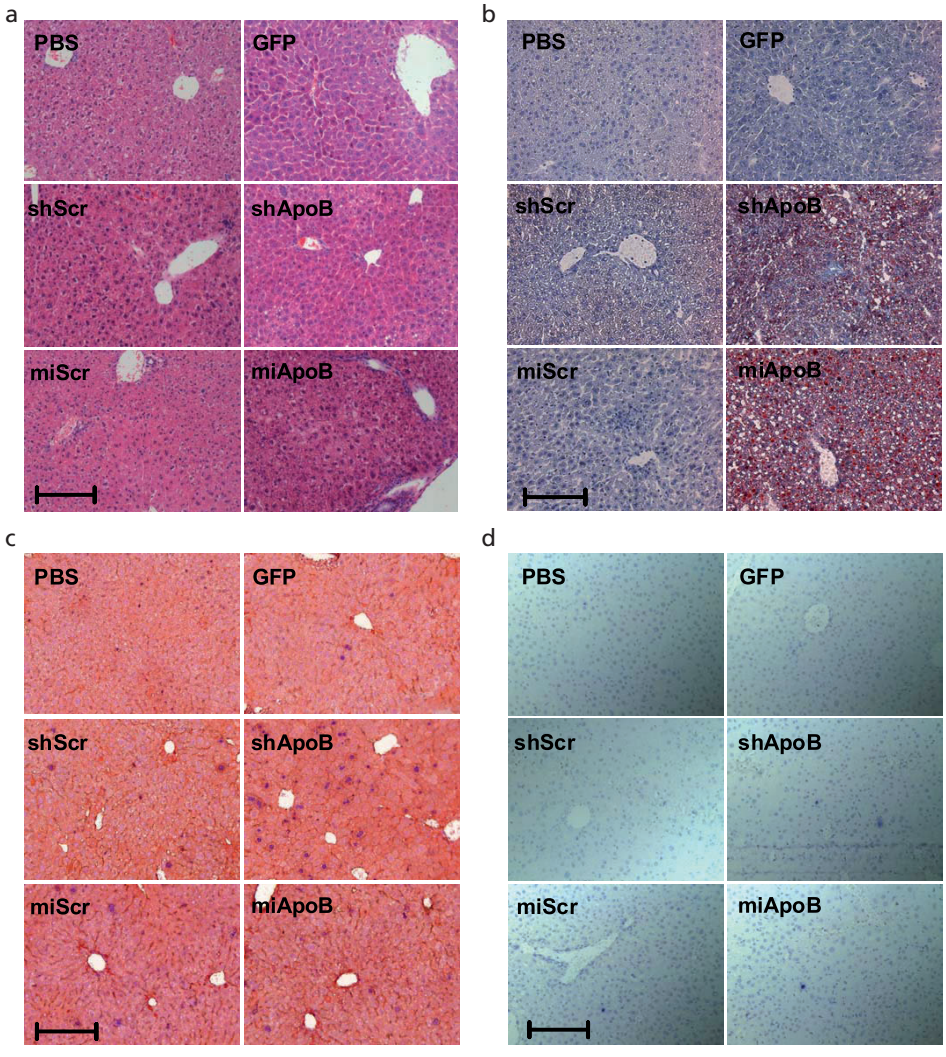
a
PBS
GFP
shScr
shApoB
miScr
miApoB
b
PBS
GFP
shScr
shApoB
miScr
miApoB
c
PBS
GFP
shScr
shApoB
miScr
miApoB
d
PBS
GFP
shScr
shApoB
miScr
miApoB
e
Proliferating hepatocytes
Number of proliferating hepatocytes
30
20
10
0
***
PBS
GFP
shScr
shApoB
miScr
miApoB

a

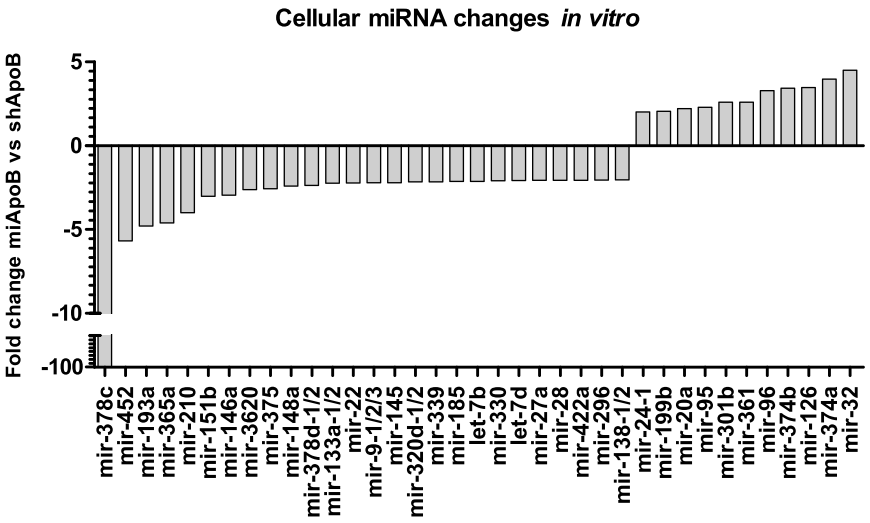

b

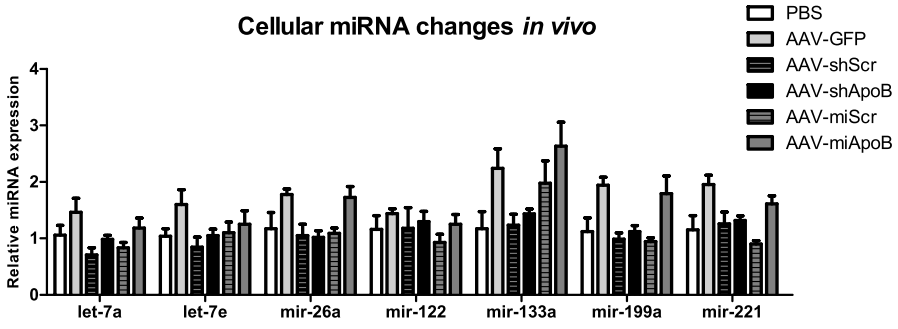

Figure 3. Effect of shApoB and miApoB expression on cellular miRNA levels *in vitro* and *in vivo.* (a) Cellular miRNA changes in miApoB vs. shApoB transfected cells. NGS analysis was performed on RNA isolated two days post-transfection with 1 µg shApoB or miApoB expression constructs. Cellular small RNA data sets were annotated to miRBase (release 18, November 2011) and grouped based on the mature miRNA sequences and reads per million (rpm) were calculated. For each miRNA, proportion of the reads and the fold change between shApoB and miApoB samples were calculated using Kal's test (Z-test) with Bonferroni correction. All miRNAs with sequential numerical identifiers up to 500 that are significantly changing are represented in the graph. (b) Verification of the NGS data *in vivo*. Relative expression of let-7a, let-7e, mir-26a, mir-122, mir-133a, mir-199b and mir-221 *in vivo* was measured by miRNA TaqMan. Mice were intravenously injected with 1×10^{11} gc AAV-shApoB or AAV-miApoB, or their respective controls AAV-shScr, AAV-miScr, AAV-GFP and PBS. Total RNA was isolated from snap-frozen livers. miRNA expression levels were calculated relative to actin mRNA and the PBS-treated group was set at 100%. Data are represented as mean ±SE, treatment groups are n = 5.

Table 2. Changes in predicted shApoB and miApoB off-target gene expression Smith-Waterman algorithm was used to predict shApoB and miApoB off-target genes for the most abundant expressed variants of passenger and guide strands in mouse reference genome (15 May 2012 NCBI build 38.1). Predicted targets were manually screened for genes expressed in the liver that were detected in NGS transcriptome analysis. For each entry the expression value RPKM and the fold change between samples relative to shScr or miScr control was calculated. If expression of a given gene in the shApoB or miApoB sample was lower than expression of the respective control sample shScr and miScr, the fold change had a negative value. ND- not detected NA-not applicable

Sequences	Strand	Targeted gene	Symbol	shApoB RPKM	miApoB RPKM	Fold change shApoB	Fold change miApoB
miApoB shApoB	guide	Apolipoprotein B (NM_009693)	ApoB	69,18	23,21	-3,1	-11,82
		Deltex 4 homolog (Drosophila) (NM_172442)	Dtx4	1,65	0,86	1,2	-1,58
		Ras responsive element binding protein 1, transcript variant 6 (NM_001177869)	Rreb1	3,63	1,87	2,4	-1,38
		Chaperonin containing Tcp1, subunit 2 (beta) (NM_007636)	Cct2	37,36	39,77	-1,2	-1,22
		Dipeptidase 1 (renal) (NM_007876)	Dpep1	0	0,59	NA	2,19
		RIKEN cDNA 2010305A19 gene (NM_027250)	2010305A19Rik	5,45	9,51	1	1,62
		PREDICTED: Uncharacterized LOC100862026 (XR_141568)	LOC100862026	ND	ND	NA	NA
miApoB	passenger	Protein kinase, AMP-activated, gamma 3 non-catatlytic subunit (NM_153744)	Prkag3	ND	0,3	NA	-2,03
		Mediator complex subunit 20 (NM_153744)	Med20	ND	5,77	NA	1,16
		A kinase anchor protein 6 (Akap6) (NM_198111)	Akap6	ND	0,01	NA	-2,35
		DNA segment, Chr 9, ERATO Doi 402, expressed (NM_001013405)	D9Ertd402e	ND	8,32	NA	1,33
		Predicted gene 4934 (NM_001167593)	Gm4934	ND	ND	NA	NA
		RIKEN cDNA 2310081J21 gene (NR_045474)	2310081J21Rik	ND	ND	NA	NA
shApoB	passenger	Regulator of G-protein signaling 12 (NM_001163512)	Rgs12	0,74	ND	1	NA
		Intraflagellar transport 52 homolog (Chlamydomonas) (NM_172150)	Ift52	10,86	ND	1,1	NA
		Budding uninhibited by benzimidazoles 1 homolog (S, cerevisiae) (Bub1), transcript variant 1 (NM_001113179)	Bub1	0,28	ND	5,8	NA
		Creatine kinase, mitochondrial 1, ubiquitous (NM_009897)	Ckmt1	0,11	ND	3,3	NA
		Tubulin tyrosine ligase-like family, member 11, transcript variant 1 (NM_029774)	Ttll11	0,11	ND	1,2	NA
		Visual system homeobox 1 homolog (zebrafish) (NM_054068)	Vsx1	ND	ND	NA	NA

NGS of liver transcriptome reveals differential gene expression in AAV-shApoB- and miApoB-injected animals

The differential siRNA processing from shRNA or miRNA scaffolds may have different consequences for induction of aspecific off-target effects. Therefore we investigated the effect of AAV-shApoB, AAV-shScr, AAV-miApoB, AAV-miScr or PBS on the liver transcriptome by performing NGS analysis. The expression abundance for each gene, represented in reads per kilobase of exon model per million mapped reads (RPKM) was calculated and Kal's test (Z-test) with Bonferroni correction was used to compare the RPKM values. We further focused on gene changes that are specific results of shApoB and miApoB expression, therefore we compared their profiles to the negative controls AAV-shScr and AAV-miScr. All AAV viruses co-expressed GFP therefore AAV-GFP sample was excluded from the NGS analysis. In the AAV-shApoB sample 106 genes were found to be significantly changed (68 were upregulated and 38 were downregulated; $p<0,05$) compared to AAV-shScr (Fig. 4a and 4b). A total of 266 genes were significantly changed ($p <0,05$) in AAV-miApoB-treated mice compared to AAV-miScr (Fig. 4a). Among them 154 genes were upregulated and 112 genes were found to be downregulated (Fig. 4b). Additionally gene expression of AAV-shApoB and AAV-miApoB samples was compared to the PBS and there was no significant difference in the amount of genes affected compared to shScr or miScr controls (Fig 4a). The number of genes affected in AAV-shApoB and AAV-miApoB samples when compared to PBS was 124 and 289, respectively (Fig. 4a). To confirm the changes observed in the NGS analysis, ApoB knockdown as measured with NGS, qRT-PCR and Western blot were compared (Fig. 4c). For both AAV-shApoB and AAV-miApoB animal groups ApoB knockdown detected with NGS correlated with qRT-PCR and Western blot data indicating that the NGS analysis is a reliable method for comparing gene expression between the different animal groups.

Next, we focused on genes that are specific results of ApoB inhibition in AAV-shApoB and AAV-miApoB-injected animals. Therefore we compared the expression of genes that are predicted to functionally interact with ApoB (Fig. 4d). Several consistently changing genes were observed like: Apobec2, Bgn and Lpl. However the majority of the ApoB-interacting genes were differentially changing between AAV-shApoB and AAV-miApoB and the expression of a number of genes remained unaltered.

Functional categorization of the NGS data

To generate a full functional profile for all genes altered by the *in vivo* expression of shScr, shApoB, miScr and miApoB, a web-based tool DAVID was used for the ontological analysis of large lists of genes (see Materials and Methods). Analysis of the 106 genes that were significantly changed in the AAV-shApoB group indicated that the most significant functional alterations were related to genes involved in lipid metabolism and

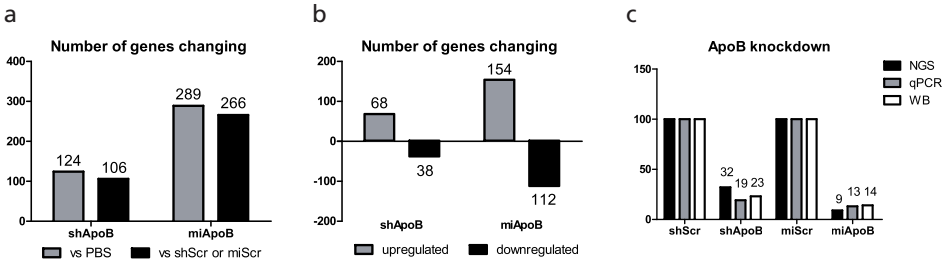

d

ApoB predicted partners' expression changes

	A1cf	Abca1	Abcg5	Acat1	ApoA1	ApoA2	ApoA4	ApoA5	Apobec1	Apobec2	Apobec3
shApoB	1,21	1,33	1,05	1,07	-1,13	-1,50	6,18	-1,20	1,77	-2,25	1,82
miApoB	-3,16	-1,95	-2,53	1,73	1,16	2,03	-8,86	-1,01	1,02	-2,50	1,32

	ApoC2	ApoC3	ApoE	ApoM	Bgn	Cd320	Cda	Ces3b	Cog2	Cyp7a1	Eif4g2
shApoB	1,56	-1,63	-1,23	-1,05	1,67	1,40	1,19	-1,68	1,54	1,76	1,26
miApoB	-1,08	1,26	1,50	1,15	1,77	2,44	1,94	1,25	1,09	1,27	-1,26

	Fgr	Hspg2	Lcat	Ldlr	Ldlrap1	Lipc	Lpl	Lsr	Mtp	Mvp	Nr1h4
shApoB	2,88	1,31	-1,35	1,23	1,66	1,08	1,88	1,02	1,21	1,48	-1,01
miApoB	1,31	-1,24	-1,31	-1,75	1,06	1,05	6,18	-1,24	-1,85	1,10	1,13

	P4hb	Pcsk9	Plg	Plk1	Pltp	Ppara	Scarb1	Sdc1	Srebf2	Txn1	Txnip
shApoB	-1,10	1,02	-1,10	4,16	1,14	1,06	1,42	1,62	1,35	-1,11	1,29
miApoB	-1,46	-2,69	-1,30	-2,07	1,03	-1,32	-1,79	1,45	-1,59	1,63	-1,09

Figure 4. NGS transcriptome analysis indicates differential gene expression profiles between AAV-shApoB- and AAV-miApoB-injected animals. To analyze liver transcriptome, total RNA was isolated from a representative animal 8 wk p.i. and NGS analysis was performed. The expression abundance for all genes was quantified using the reads per kilobase of exon model per million mapped reads (RPKM) measure. Expression data was compared using Kal's Z-test with Bonferroni correction. Genes significantly altered ($p<0,05$) were used in further analysis (a) Genes significantly altered ($p<0,05$) in AAV-shApoB- and AAV-miApoB-injected animals. Grey bars represent gene changes compared to PBS group and black bars represent gene changes compared to AAV-shScr or AAV-miScr controls (b) Genes significantly upregulated or downregulated in AAV-shApoB and AAV-miApoB injected animals. Grey and black bars represent number of genes upregulated and downregulated respectively compared to AAV-shScr or AAV-miScr controls ($p<0,05$) (c) Comparison of ApoB knockdown *in vivo* by NGS, qRT-PCR and protein Western blot. In all assays ApoB expression levels were calculated relative to AAV-shScr or AAV-miScr, which served as negative controls and were set at 100%. (d) Prediction of ApoB functional interactions was performed with STING software. Upregulated genes (fold change > 1,5) were marked in green and downregulated (fold change < -1,5) were marked in red.

transport and response to stimuli (Fig. 5a). In addition, expression of genes involved in drug metabolism, inflammation, cell growth and death and the MAPK signaling pathway were altered. In the AAV-miApoB animal group, the 266 significantly altered genes corresponded mainly to genes involved in drug metabolism, oxidoreductase activity and processes (Fig 5b). Other relevant pathways include lipid metabolism and transport, ion binding, response to stimuli and nucleobase, nucleoside and nucleotide biosynthetic process. A complete list of genes functionally annotated with DAVID

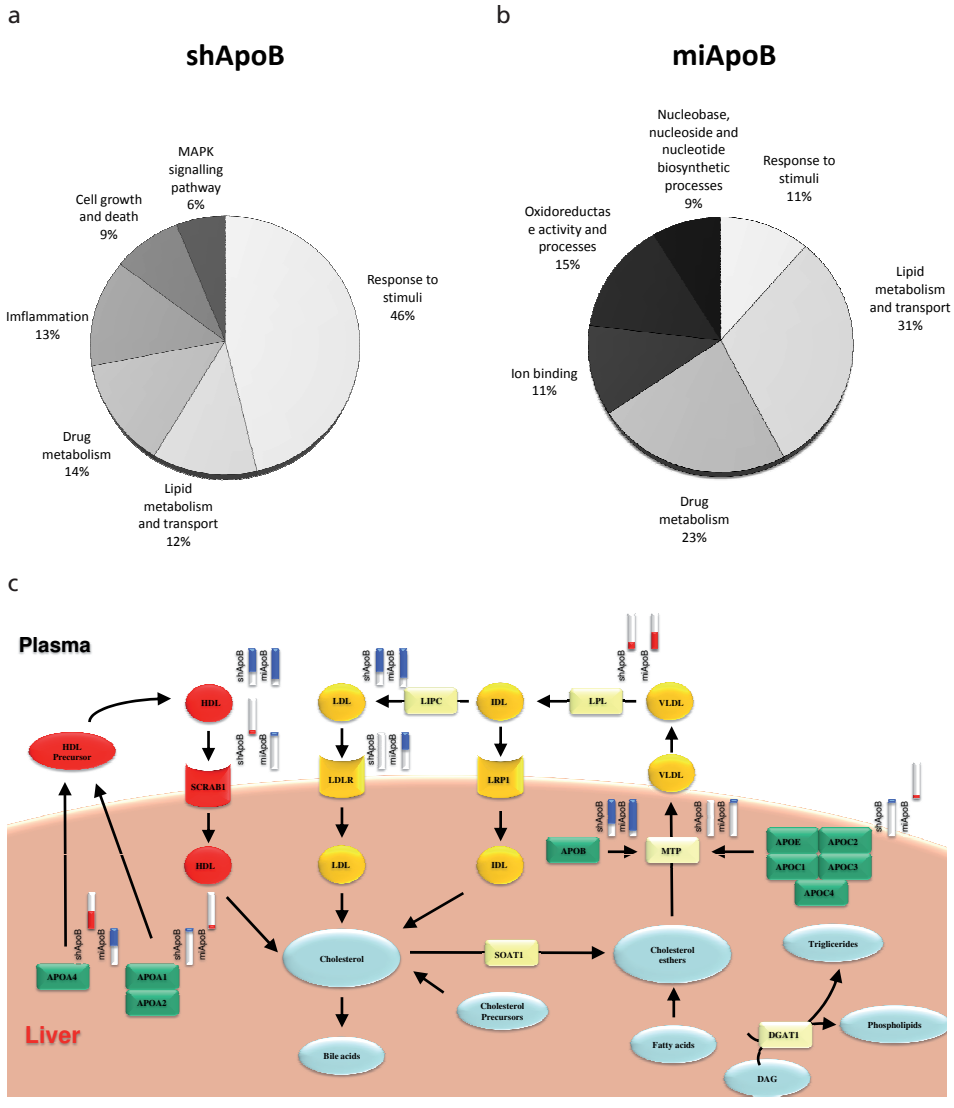

Figure 5. Functional categorization of gene expression changes in AAV-shApoB and AAV-miApoB injected animals. (a) Percentage and functional categorization of genes significantly changing in AAV-shApoB and AAV-miApoB animal groups. Genes significantly altered in AAV-shApoB and AAV-miApoB groups ($p<0,05$) were annotated to Gene Ontology (GOTERM_BP_FAT and GOTERM_MF_FAT) and KEGG (KEGG_PATHWAY) using the Database for Annotation, Visualization and Integrated Discovery (DAVID) v6.7 (National Institute of Allergy and Infectious Diseases (NIAID), NIH). Significant annotations ($p<0,05$) were grouped in 8 categories and the percentage of genes in each category was calculated with reference to all genes annotated in the DAVID analysis.(b) Outline of cholesterol pathway changes in AAV-miApoB and AAV-shApoB injected animals. There are several types of lipoproteins within blood: chylomicrons, very-low-density lipoprotein (VLDL), intermediate-density lipoprotein (IDL), low-density lipoprotein (LDL), and high-density lipoprotein (HDL). ApoB100 protein is synthesized in the liver and it forms the structural protein in VLDL and LDL particles. HDL is secreted by the gut and liver and receives additional components during the ►

► metabolism of triglyceride-rich lipoproteins. Therefore inhibition of ApoB affects VLDL-C, LDL-C and HDL levels-C. Genes significantly altered in the AAV-shApoB and AAV-miApoB groups were used ($p<0,05$) for toxicology prediction using Metacore software (Thomson Reuters) and the top scored map was generated. Experimental data from AAV-shApoB and AAV-miApoB groups are linked to and visualized on the image as thermometer-like figures place in the top right of respective gene or group of genes. Upward red colored thermometers indicate up-regulated components and downward blue thermometers indicate down-regulated components of the pathway.

for miApoB and shApoB samples can be found in Supplementary Tables 3 and 4, respectively. Although both shApoB and miApoB resulted in the same phenotypic effect as result of ApoB knockdown, the changes exerted on other lipid metabolism genes were rather dissimilar (Fig. 5c). Inhibition of ApoB in AAV-shApoB-injected mice resulted in a decrease of LDL-C and HDL-C associated genes: ApoA2, ApoE, ApoC1, ApoC3 and ApoC4. By contrast the same genes were upregulared in AAV-miApoB-injected samples. Furthermore miApoB was associated with downregulation of ApoA4, Ldlr, Pcsk9 and Scarb1, which are key components in cholesterol homeostasis. By contrast, ApoA4 and Scrab1 genes were upregulated in the AAV-shApoB sample. In both AAV-shApoB- and AAV-miApoB-injected animals Apobec2 gene was downregulated while Lpl gene was significantly upregulated (Fig 5c).

Although both shApoB and miApoB were found to affect response to stimuli and drug metabolism, only the serine protease inhibitors Serpina1b, Serpina1c, Serpina1d and Serpina3k were simultaneously affected in both groups. Serpins compose a large family of the functional diverse proteins which are involved in numerous intracellular and extracellular functions: blood clotting, inflammation, storage, hormone carriage and tumor suppression [29-31]. Only AAV-shApoB injection was found to upregulate genes involved in inflammatory response such as Serpina 8N which is induced during inflammation and Serum amyloid A1 (Saa1), a major acute phase reactant. shApoB but not miApoB expression also upregulated components of the MAPK signaling pathway: Fos, Jun, Nr4a1, Dusp1 and Dusp6. Fos, Jun, Nr4a1 are transcription factors involved a number of cellular processes including differentiation, proliferation, and apoptosis [32] and Nr4a1 plays a key role in mediating inflammatory responses in macrophages [33]. Dusp1 and Dusp6 negatively regulate the members of the MAPK family pathways JNK and p38, which results in cell apoptosis [34].

miApoB expression downregulated genes involved in drug metabolism such as members of alpha-glutathione-S-transferase Gsta1, Gsta2, Gsta4 and glutathione-S-transferase mu genes Gstm1, Gstm2, Gstm3 and Gstm3. By contrast, expression of those genes was upregulated in the AAV-shApoB-injected animal. Other genes that were upregulated in AAV-miApoB-injected animal are involved in oxidoreductase activity, oxidative phosphorylation and nucleic bases biosynthetic processes. Most of these are structural components of mitochondrial oxidative phosphorylation system: NADH-coenzyme Q oxidoreductase (complex I), Cytochrome bc1 complex

(complex III), Cytochrome c oxidase (complex IV) and ATP synthase (complex V). Finally, genes involved in lipid metabolism and transport that encode alcohol dehydrogenase (Adh1), Acetyl-Coenzyme A acyltransferase (Acaa1b, Acaa1a, Acaa2), Aldehyde dehydrogenase 3 family (Aldh3a2) and Cytochrome P450 family members (Cyp4a10, Cyp3a11, Cyp2c29, Cyp4a14) were upregulated in the AAV-miApoB sample.

shApoB and miApoB do not affect the expression of predicted off-target genes

A common source of RNAi toxicity is off-targeting, when non-targeted transcripts are down-regulated as a consequence of sequence complimentarily to the shRNA or miRNA sequence. In our previous study we have shown that shApoB and miApoB are differentially processed *in vivo* and that a pool of different guide and passenger strands was generated. To investigate possible off-target effects, the Smith-Waterman algorithm was used to predict the most abundant guide and passenger strand variants (Table 2). A total of 19 genes were predicted as off-targets in the liver for the guide and passenger strand of shApoB and 25 for miApoB. To investigate if any of the predicted interactions correlates with our experimental data, *in vivo* NGS data was manually screened for the predicted off-target gene expression and evaluation of the changes was performed (Table 2 and Fig. 6). From the 19 predicted off-target genes, 11 were expressed in AAV-shApoB animals and 10 in AAV-miApoB-injected animals. Surprisingly, the expression of none of the predicted off-targets for both shApoB and miApoB was significantly changed *in vivo* (Table 2 and Fig 6).

5 Discussion

The major challenge for the RNAi-based therapies is the delivery of siRNAs to the target tissue or organ for stable and long-term inhibition of a disease-related gene. Recent reports on the RNAi toxicity have initiated a discussion about the safety of such an approach. Although in the last few years much progress has been made in understanding the causes of toxicity and approaches to preclude adverse effects have been suggested, detailed studies on the differences between shRNA- or artificial miRNA-encoding constructs and the consequences for *in vivo* applications have not been reported. By using AAV delivery, we have compared the safety profiles of identical predicted siApoB sequences expressed as shApoB and miApoB in long-term *in vivo* studies. Detailed histological analyses, as well as comparison of endogenous miRNA and transcriptome expression revealed major differences between AAV-shApoB- and AAV-miApoB-injected animals, indicating that careful monitoring is necessary prior to proceeding clinical trials.

In vivo toxicity of shRNA was often linked to upregulation of liver enzymes ALT and AST in mice [8,10] and in non-human primates [35]. In our experiment, transient activation of liver transaminases was observed in AAV-miScr and AAV-miApoB animals

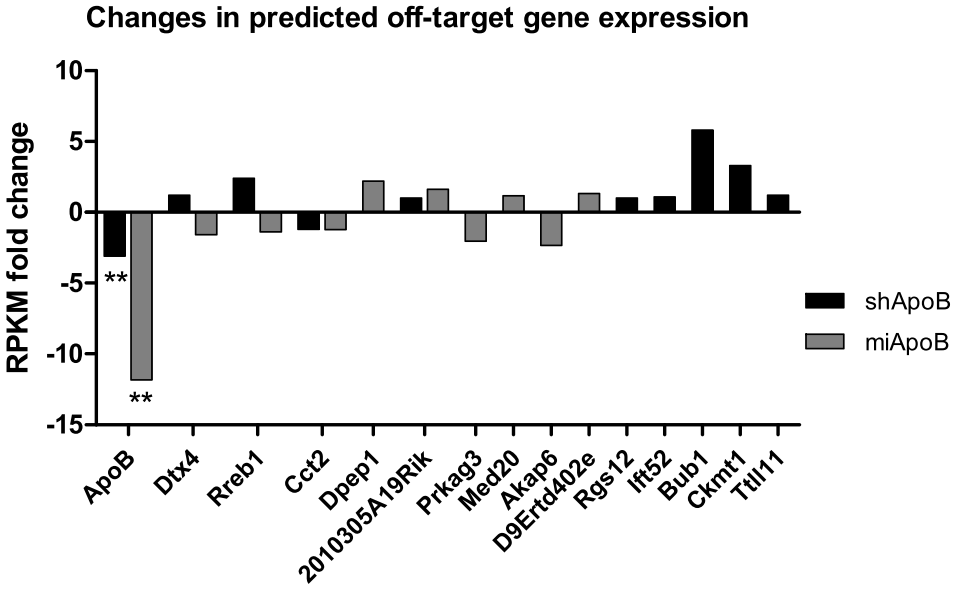

Figure 6. Changes in predicted shApoB and miApoB off-target gene expression. Smith-Waterman algorithm was used to predict shApoB and miApoB off-target genes for the most abundant expressed variants of passenger and guide strands in mouse reference genome (15 May 2012 NCBI build 38.1). Predicted targets were manually screened for genes expressed in the liver that were detected in NGS transcriptome analysis. Grey and black bars represent fold change in AAV-shApoB and AAV-miApoB relative to AAV-shScr or AAV-miScr controls respectively. Kal's test (Z-test) with Bonferroni correction was used to compare the RPKM value in the shApoB versus shScr or miApoB versus miScr. $^{**}p < 0.01$

during the course of the experiment indicating mild dose-dependent toxicity. We have previously reported that such toxicity can be abolished by lowering the administered viral dose [24]. In contrast to our results, Ahn *et al.* described increased in ALT levels 3 weeks p.i. after injection of adenovirus encoding shRNA against transcription factor Srebp1 and lipid transporter Fatbp5 [7]. Interestingly in their study, scrambled control hairpin did also cause increase in ALT levels, indicating that toxicity was associated with shRNA expression and was not due to adenoviral vector. This also suggests that shRNA liver toxicity is probably sequence-dependent. In another study, three-fourths of the tested shRNAs resulted in liver injury, while expression of others was well tolerated [10]. Although transient ALT and AST increase was detected in AAV-miScr- and AAV-miApoB-injected animals, no acute inflammation and no gross-changes of liver morphology in these groups were detected.

Similar to previous studies, ApoB knockdown by AAV-shApoB and AAV-miApoB resulted in hepatic fat accumulation [36,37]. Surprisingly steatosis was not observed in murine studies with an ApoB antisense oligonucleotide [38]. By contrast, clinical trials with the human ApoB antisense oligonucleotide did reveal a trend toward an

increase in intrahepatic triglyceride content [39]. Steatosis may be associated with inflammation and may progress to cirrhosis, therefore careful consideration and investigation of this consequence of lowering ApoB is necessary. Tep *at al.* reported that simultaneous silencing of Mtp and Dgat2 rescues siRNA-induced hepatic steatosis [48]. However Dgat2 silencing resulted in a significant increase of plasma ketones making this approach not attractive for clinical applications as elevated serum ketones can cause medical emergency. By contrast, double knockdown of ApoB and Dgat2 or Fabp5 did not result in reduction of lipid accumulation.

We observed that injections of AAV-shApoB, but not AAV-miApoB, caused increased hepatocyte proliferation. The reason for the observed proliferation would be hepatocyte damage due to RNAi-induced toxicity. Increased apoptotic and proliferative activity has been observed in murine liver expressing AAV-delivered shRNA targeting human alpha-1-antitripsin [10] and adenoviral-expressed targeting Srebp1 and Fabp5 [7]. In our experiments we observed increased proliferation that was not associated with apoptosis, implying that apoptosis may have occurred earlier than 8 wk p.i. with AAV-shApoB. Another reason for the increased proliferation could be the hepatic steatosis. Indeed, It has been reported that increase in liver triglycerides may lead to increased oxidative stress in the hepatocytes and lipid-activated apoptosis [40]. The fact that miApoB does not affect liver proliferation excludes this possibility. Based on our data and previous reports, we can only conclude that increased liver proliferation due to shApoB expression is hairpin structure- and concentration-specific. It should be noted that AAV-miApoB- and AAV-miScr-injected animals did not reveal signs of increased liver proliferation, which could have important consequences for long-term correction, since AAV DNA forms episomal nuclear concatamers in the host cell nucleus, which are lost following cell division [41]. Those results also explain our previous observations where the silencing effect in AAV-shApoB-injected animals was less sustained than in AAV-miApoB-injected animals [24].

Saturation of the RNAi pathway and global de-regulation of endogenous miRNA processing as a consequence of overexpression of hairpin structures play an important role in RNAi-induced toxicity [8,10]. Castanotto *et al.* showed that both siRNAs and shRNAs against the HIV regulator gene Rev competed with the endogenous mir-21 expression *in vitro* in HEK293T cells [42]. However the siRNA sequences used in that setting did not show competition with endogenous miRNA when expressed as artificial miRNA. In another study mir-21 was shown to be affected by expression of artificial miRNA against the hepatitis virus B (HBV) genome in Huh7 cells [43]. The competition with endogenous miRNA was dose-dependent as potent silencing was also achieved with lower doses where RNAi saturation was not observed. It has also been reported that shRNA-induced toxicity resulted in inhibition of mir-122 and let-7a *in vitro* and *in vivo* [8,10]. Our NGS analysis of small RNA profiles showed significant divergence between shApoB- and miApoB-transfected cells. *In vivo* of 7 tested miRNAs only

mir-133a was differentially expressed in the AAV-miApoB-injected group compared to AAV-shApoB-injected group. However we cannot exclude that complete NGS profiling of miRNA expression *in vivo* would allow identification of other differentially expressed endogenous miRNAs. Importantly in both *in vitro* and *in vivo* experiments, we did not observe global downregulation of endogenous miRNA expression indicating that therapeutic delivery of AAV-shApoB and AAV-miApoB did not induce toxic effects.

The NGS analysis of liver transcriptome revealed differential gene expression in AAV-shApoB- and AAV-miApoB-injected animals. As anticipated, lipid metabolism and transport genes were affected for both molecules. Interestingly, Bgn, a proteoglycan which can bind ApoB-containing lipoproteins and is involved in atherosclerosis [44], and Lpl is one of the key enzymes for lipoprotein catabolism which hydrolyzes triglycerides and VLDL-C [45], were upregulated for both AAV-shApoB and AAV-miApoB. In addition to lipolysis, Lpl mediates the uptake and degradation of lipoproteins by cells. Our hypothesis is that the upregulation of these two genes might be a compensatory reaction to the strong ApoB decrease in murine liver but the biological significance of those changes needs to be determined. Apobec2, which is an ApoB mRNA editing enzyme, was downregulated in both treatment groups probably as a result of the low concentrations of ApoB in the liver of shApoB and miApoB animals. Although Abobec2 functions in liver are not fully investigated, its upregulation has been associated with tumorogenesis and development of hepatocellular carcinoma through hepatic inflammation [46]. By contrast Apobec2 deficient mice did not reveal any abnormalities on health and survival [47].

Surprisingly, the majority of the lipid metabolism genes were differentially affected in AAV-shApoB and AAV-shApoB animals despite the same phenotypic effect. Recently, significant changes in many lipid metabolism genes following ApoB silencing with siRNA have been reported using TaqMan analysis [48]. Out of 96 genes which were investigated, 53 were downregulated more than 1,5 fold while only 7 were upregulated. However when compared to our NGS data, only a few genes had a similar change in expression profile (Table S5). This may suggest that siRNA, shRNA and miRNA induce different gene expression profile despite the same phenotypic effect. However, it has to be noted that the siApoB used had a different sequence and the experiment was performed in LDL-R/CETP+/- hemizygous mice, which exhibit different lipid profile. Additionally the analysis was performed 2 wk p.i. with siApoB and at this time point gene expression changes may have been more pronounced. To our knowledge comparison of liver gene expression analysis after siRNA, shRNA and miRNA administration has not been performed.

Besides lipid metabolism and transport other functions were also altered in murine liver by expression of AAV-shApoB or AAV-miApoB. Response to stimuli and drug metabolism were found to be affected in both shApoB and miApoB groups, but the genes involved showed minimal overlap. shApoB was found to affect genes involved

in cell growth and death, inflammation and MAPK pathway, which correlated with our findings on increased liver proliferation. miApoB affected genes involved in ion binding, nucleobase biosynthetic process and oxidative activity and processes. Previously, Ahn *et al.* described significant transcriptomic changes in mice after adenoviral deliver of shRNA [7], where a total number of 181 genes, were found to be upregulated while only 32 genes were found to be downregulated as a consequence of shRNA expression. Data generated from their study suggested that shRNA expression also upregulated genes involved in the RNAi pathway and proliferation. In contrast, we did not see significant upregulation of those genes, which might be due to the fact that we performed our analysis 8 weeks p.i. and because we used AAV as a delivery vector. Importantly we detected upregulation of inflammatory related genes exclusively in the AAV-shApoB group although no signs of inflammation in the liver could be found and in our previous experiments we did not measure IFN response activation [49]. Immune activation might indeed have caused hepatocytes' damage in the AAV-shApoB sample resulting in increased proliferation and eventually loss of the knockdown effect. The consequences of the activation of genes involved in immune response solely by AAV-shApoB needs to be further investigated by careful monitoring their expression over time and when different shRNAs and AAV doses are used.

Another important observation was that none of the changes in gene expression in AAV-miApoB and AAV-shApoB resulted from aspecific down-regulation of off-target transcripts. Although we could not explain the changes in gene expression by off-target prediction using the Smith-Waterman algorithm, we cannot exclude that some of the interaction may have been missed and other prediction methods like screening 3' UTRs of genes for perfect complementarity to siRNA seed region may be more accurate. miRNAs may regulate their targets by translational repression, therefore we might speculate that the off-target effects may be stronger at protein level.

In summary, our findings demonstrate that the incorporation of identical siRNA sequences in shRNA or artificial miRNA scaffolds induces differential effects on liver morphology, transcriptome and cellular miRNA expression. Despite effective silencing, same phenotypic effect and no signs of severe toxicity, multiple genes and functions were de-regulated by AAV-shApoB or AAV-miApoB. Mir-133a was upregulated in AAV-miApoB animals and might be one of the mediators responsible for the observed differences between shApoB and miApoB. Furthermore only expression of shApoB resulted in increased hepatocyte proliferation indicating the miApoB is a better candidate for future development of RNAi therapeutics of familial hypercholesterolemia. Finally, miApoB expression was limited to the liver due to the use of a tissue-specific promoter, while the presence of shApoB-derived siApoB was detected in spleen, heart, lung, kidney, and ileum. All those features of AAV-miApoB makes us consider the use of tissue-specific expression of therapeutic siRNA from miRNA scaffolds a safer option than shRNA.

Materials and methods

DNA constructs AAV production and purification

The design and cloning of the shApoB, shScr, miScr, miApoB and GFP expression vectors, scAAV8 vector production and purification has been described previously [24,49].

In vivo experiments

All animal experiments were conducted according to the guidelines of the local animal welfare committee. Six-to-eight-week-old male C57BL/6 mice received an intravenous AAV injection of 1×10^{11} gc per animal (~4×10^{12} gc/kg) via the tail vein. Treatment groups were n=5, mice were housed 6 per cage and feeding was performed *ad libitum* with regular chow. Heparinized blood samples were taken every two weeks p.i. from fasted mice. Mice were sacrificed at 8 weeks p.i. and liver and plasma were collected for analysis. Plasma levels of ALT, AST, and total cholesterol were analyzed on the automated clinical chemistry analyzer Modular Analytics P800 (Roche Diagnostics, Basel, Switzerland) at the Academic Medical Center (Amsterdam, the Netherlands). Statistical analysis was performed by ANOVA testing with Bonferroni post test and $p<0.05$ was considered significant.

GFP expression was analyzed in snap-frozen liver sections. Livers were cryosectioned at 5 µm and eGFP signal was visualized using standard fluorescence microscopy on a Leica fluorescent microscope (Leica Microsystems GmbH, Wetzlar, Germany). For analysis of liver fat accumulation, snap-frozen liver sections were cryosectioned at 5 µm, fixed in 10% formalin and stained for 25 min in filtered 0.3 % Oil red O (Sigma, St. Louis, MO) solution in 60% isopropanol. Nuclei were counterstained for 5 min in hematoxylin solution (Sigma, St. Louis, MO). Liver histology was assessed by hematoxylin-eosin (H&E) staining of frozen liver sections.

Immunohistochemistry

Mouse liver samples were fixed with buffered 4% formalin (NBF) for 48 h and then routinely processed to paraffin blocks. Five-micrometer sections were cut, mounted on coated slides and dried overnight at 37°C. Slides were dewaxed in xylene and hydrated with the use of graded alcohols to tap water. Endogenous preoxidases were blocked by incubation in methanol supplemented with 0,3% peroxide. Heat induced endogenous antigen retrieval (HIER) was performed in the PreTreatment Module (PTModule; Thermo Fisher Scientific/Labvision, Fremont, CA) for 20 min at 98°C and a cool-down to 75°C in Tris-HCI + EDTA pH 9.0. After washing sections with running tap water, Ultra V Block (Thermo Fisher Scientific/Labvision, Fremont, CA) for 10 minutes at room temperature (RT). A sequential triple staining procedure [50] started with CD31 (LifeSpan Biosciences Inc., Seattle, WA) visualized by horseradish peroxidase (HRP) conjugated anti-rabbit IgG polymer and BrightDAB (both Immunologic, Duiven, The Netherlands). The DAB reaction product effectively shelters the first set of

antibodies and thus prohibits unwanted cross-reactions with later incubation steps. Staining was continued with anti-Ki67, clone SP6 (Thermo Fisher Scientific/Labvision, Fremont, CA) visualized by BrightVision alkaline phosphatase (AP) conjugated anti-rabbit IgG polymer (Immunologic, Duiven, Then Netherlands) and Vector Blue (Vector Laboratories, Burlingame, CA, USA). Next, a second HIER step (10 min, 98C) using citrate buffer pH6. 0 was applied to remove all antibodies used but leaving the chromogens unchanged. Finally, CK18 (Abcam, Cambridge, UK) was visualized by BrightVision AP conjugated anti-mouse IgG polymer (Immunologic) and Vector Red (Vector Labs). Slides were weakly counterstained with hematoxylin diluted 1:5 in distilled water for 3 min, washed with tap water, completely dried at a hot plate and non-aqueous coverslipped with VectaMount (Vector Labs). Primary and secondary antibodies used in this study are listed in Table 1. Antibodies and conjugates were diluted in antibody dilutent (Immunologic) and Tris-buffered saline (TBS) was used as washing buffer for all further steps (three changes, 3 min each). HRP activity in brown was developed with Bright DAB (Immunologic) according to manufacturer's instructions. Alkaline phosphatase (AP) activity in blue and in red was developed with the Vector Blue and Vector Red kits (Vector Laboratories, Burlingame, CA) with the use of a Tris-HCI buffer (100 mM, pH 8.2) according to manufacturer instructions.

Spectral Imaging and proliferation quantification

Specimens were observed with a Leica BM5000 microscope equipped with plan apochromatic objectives (Leica Microsystems, Wetzlar, Germany). From all IHC triple stained slides, multispectral data sets of five random fields with Ki67 positive nuclei at 200x were acquired using a Nuance imaging system (PerkinElmer/Caliper Life Science, Hopkinton, MA). Spectral libraries were created acquiring spectra from 420-720 nm at 20 nm intervals from single-staining with DAB, Vector Blue, Vector Red and Hematoxylin. Spectral data sets from triple staining and control slides were acquired at the same wavelengths. To analyze the frequency of proliferating hepatocytes, MSI data sets were analyzed with InForm 1.4 image analysis software (PerkinElmer/Caliper Life Science) as earlier described for proliferating hepatocytes in rabbit liver by Van der Loos *et al.* [50]. The learn-by-example interface from the software segments hepatocytic and sinusoidal tissue compartments. Next, the number of proliferating hepatocytes by analyzing the number of cells in the hepatocytic tissue compartment with co-expression for cytoplasmic CK18 (Vector Red) and nuclear Ki67 (Vector Blue) was calculated. For comparison and validation of the automated procedure, two observers independently manually counted all Ki67-positive hepatocytes in the images which were used to create the algorithm.

Western blot analysis for detection of ApoB100 protein

Murine plasma proteins from 8 wk p.i. (0.1 µl) were separated by electrophoresis on a 3–8% Tris-Actetate gel (Invitrogen) and blotted onto a 0.45-µm nitrocellulose

membrane (Invitrogen). The blot was incubated with a 1:2,000 dilution of a rabbit polyclonal anti-ApoB antibody (ab31992; Abcam, Cambridge, UK), followed by incubation with a 1:2,000 dilution of goat anti-rabbit antibody conjugated to horseradish peroxidase (P0448; Dako, Glostrup, Denmark). Antibody binding was detected by the Lumi-LightPLUS chemiluminescent detection kit (Roche Diagnostics, Basel, Switzerland). Equal loading of protein samples was confirmed by Ponceau S staining (Sigma, St Louis, MO).

Cell culture and transfections

The human embryonic kidney 293T (HEK293T) cell line was maintained in Dulbecco's modified Eagle's medium (DMEM; Invitrogen, Carlsbad, CA) containing 10% fetal calf serum, 100 U/ml penicillin and 100 U/ml streptomycin, at 37°C and 5% CO_2. For small RNA next generation sequencing (NGS) cells were seeded in 6-well plates at a density of 4.5×10^5 cells per well in DMEM one day prior transfection. Transfections were performed with Lipofectamine 2000 reagent (Invitrogen, Carlsbad, CA) according to the manufacturer's instructions. RT reactions for siApoB expression *in vivo* and let-7a, let-7e, mir-26a, mir122, mir-133a, mir-199a and mir-221 expressions *in vitro* were performed with the TaqMan MicroRNA Reverse Transcription Kit (Applied Biosystems, Foster City, CA) using 10 ng RNA and 3 µl custom-made specific RT-stem-loop primer (Applied Biosystems, Foster City, CA) according to the manufacturer's instructions. Amplification of the beta actin gene was used as a RNA quality and loading control. siApoB copy number per cell was calculated based on the amplification plot of a dilution series of synthetic siApoB RNA standard (IDT, Coralville, IA). The trend line value of the standard line was used to calculate the siApoB copy number cell, assuming 15 pg RNA per cell [51]. Let-7a, let-7e, mir-26a, mir122, mir-133a, mir-199a and mir-221 levels were normalized to β-actin and the relative gene expression $2^{-\Delta\Delta Ct}$ method of Livak and Schmittgen was used for analysis of PCR data [52].

RNA isolation, quantitative real-time RT-PCR (qRT-PCR), siRNA and miRNA Taqman assay

To determine ApoB mRNA knockdown and siApoB expression *in vivo* , total RNA was isolated from frozen liver sections at 8 weeks p.i. using Trizol (Invitrogen, Carlsbad, CA). Genomic DNA (gDNA) was removed by DNase treatment using TURBO DNase (Ambion, Austin, TX). First strand cDNA was reverse transcribed using random hexamer primers with the Dynamo kit (Finnzymes, Espoo, Finland). Real time PCR amplification was performed with ApoB- and beta actin-specific primers. PCR reaction conditions were: 95°C for 10 min, followed by 40 cycles of 15 sec at 95°C and 1 min at 60°C. The assays were performed on ABI 7000 or ABI 7500 (Applied Biosystems, Foster City, CA). ApoB expression levels were normalized to beta actin as an internal control, and the relative gene expression $2^{-\Delta\Delta Ct}$ method of Livak and Schmittgen was used for analysis of PCR data [52].

Next Generation Sequencing (NGS) of small RNA and liver transcriptome

For NGS analysis of small RNA, HEK293T cells were transfected with 4 µg shApoB- or miApoB-expression plasmids using Lipofectamine 2000 reagent and total RNA was isolated from cells 48 hr post-transfection using Trizol (Invitrogen, Carlsbad, CA) according to the manufacturer's protocol. Small RNA sequencing libraries were generated using high-quality total RNA as input and the NEXTflex Small RNA Sequencing kit (Bioo Scientific, USA). Briefly, the small RNA species were subjected to ligation with 3' and 5' RNA adapters, first strand reverse transcription, and PCR amplification. Sample-specific barcodes were introduced in the PCR step. The PCR products were separated on TBE-PAGE electrophoresis and the expected band around 140-160bp was recovered for each sample. The resulting sequencing libraries were quantified on a BioAnalyzer (Agilent). The libraries were multiplexed, clustered, and sequenced on an Illumina HiSeq 2000 (TruSeq v3 chemistry) with a single-read 36 cycles sequencing protocol and indexing. The sequencing run was analyzed with the Illumina CASAVA pipeline (v1.8.0), with demultiplexing based on sample-specific barcodes. The raw sequencing data produced was processed removing the sequence reads which were of too low quality (only "passing filter" reads were selected), and discarding reads that aligned against the PhiX control. In total, we generated 16016701 reads for sample miApoB, and 15843150 reads for sample shApoB. The NGS small RNA raw data set was analyzed using the CLC_bio genomic workbench (CLC Bio, Aarhus, Denmark). The obtained reads were adaptor-trimmed, which decreased the average read size from ~36bp to ~25bp. The custom adapter sequenced used for trimming all the bases extending 5' was: GTGACTGGAGTTCCTTGGCACCCGAGAATTCCA. All reads containing ambiguity N symbols, reads shorter than 15 nt, longer than 55 nt in length and reads represented less than 10 times were discarded. To relatively represent the expression counts for the small RNAs obtained in the experiment, reads per million (rpm) or percentage of reads based on the total number of reads matching the reference shApoB or miApoB sequence were calculated Finally, to identify the differences in cellular miRNA reads between the miApoB and shApoB samples the small RNA data sets were annotated to miRBase, Release 18 and grouped based on the mature miRNA sequences, the rpm were calculated and the fold change between miApoB and shApoB samples was calculated.

To analyze liver transcriptome, total RNA was isolated from frozen liver sections of representative animals at 8 weeks p.i. with AAV-shApoB, AAV-miApoB, AAV-shScr, AAV-miScr or PBS using Trizol (Invitrogen, Carlsbad, CA). RNA sequencing libraries for the Illumina sequencing platform were generated using high-quality RNA as input and the Illumina TrueSeq RNA v2 Sample preparation kit. Briefly, poly-A containing mRNA molecules were purified using poly-T oligo-attached magnetic beads. Following purification, the mRNA was fragmented via incubation for 5 min at 94°C with the

Illumina-supplied fragmentation buffer. The first strand of cDNA was next synthesized by reverse transcription using random oligo primers. Second-strand synthesis was conducted by incubation with RNase H and DNA polymerase I. The resulting double-stranded DNA fragments were subsequently endrepaired, and A-nucleotide overhangs were added by incubation with Taq Klenow lacking exonuclease activity. After the attachment of adaptor sequences, fragments were PCR-amplified using Illumina-supplied primers. The resulting sequencing libraries were quantified on a BioAnalyzer (Agilent). The libraries were multiplexed, clustered, and sequenced on an Illumina HiSeq 2000 (TruSeq v3 chemistry) with a single-read 36 cycles sequencing protocol and indexing. The sequencing run was analyzed with the Illumina CASAVA pipeline (v1.8.0), with demultiplexing based on sample-specific barcodes. The raw sequencing data produced was processed removing the sequence reads which were of too low quality (only "passing filter" reads were selected), and discarding reads that aligned against the PhiX control. Each read file (sample), in the FASTQ format, was individually aligned against the Mouse reference genome (15 May 2012 NCBI build 38.1) using CLC Bio- Genomic Workbench. The expression abundance for all genes was quantified using the reads per kilobase of exon model per million mapped reads (RPKM) measure [53]. Expression data was compared using Kal's Z-test with Bonferroni correction. Smith-Waterman algorithm was used to predict off-target genes in Mouse reference genome (15 May 2012 NCBI build 38.1) for the most abundant expressed variants of both passenger and guide strands of shApoB and miApoB. Small RNA and transcriptome NGS was carried out by Macrogen Inc. (Seoul, Korea).

The NGS data discussed in this publication have been deposited in NCBI's Gene Expression Omnibus [54] and are accessible through GEO Series accession number GSE39187 (http://www.ncbi.nlm.nih.gov/geo/query/acc.cgi?acc=GSE39187).

Functional analysis

For the ApoB functional interactions, online database resource search tool for the retrieval of interacting genes (STRING) was used, which allowed annotation of functional interactions of ApoB protein in cell (http://string-db.org/) [55]. For the genes that were identified RPKM gene expression values were compared to PBS or shScr and miScrand and fold change between sample and control was calculated. Upregulation of genes (fold change > 1,5) was marked in green and downregulations (fold change < -1,5) were marked in red.

For the transcriptome analysis, RPKM gene expression values were compared to PBS using Kal's test (Z-test) with Bonferroni correction. All genes that changed significantly ($p<0,05$) and were expressed higher than 0,1 (RPKM>0,1) were included in the further analysis. Functional analysis of the significantly changing genes was done with the functional annotation tool DAVID (Database for Annotation, Visualization and Integrated Discovery v6.7; National Institute of Allergy and Infectious Diseases,

NIH) that allows finding combination of genes under study with respect to a reference list [56,57]. The annotations were done simultaneously with the reference to Gene Ontology databases (GOTERM_BP_FAT and GOTERM_MF_FAT, www.geneontology.org) and to KEGG pathway database (KEGG_PATHWAY; www.genome.ad.jp/kegg/pathway.html). The redundancy in the gene list was manually analyzed and significant annotations were grouped in 8 categories and the percentage of genes in each category was calculated with reference to all genes that were annotated in DAVID analysis.

Supplementary material

Table S1. Description of histological scoring system of liver morphology

Macrovesicular steatosis Grade	<5% 5%-33% 34%-66% >67%	0 1 2 3
Microvesicular steatosis grade	<5% 5%-33% 34%-66% >67%	0 1 2 3
Ballooning Grade	none few cells prominent ballooning	0 1 2
Lobular Inflammation assessment of all foci per 10x objective	no foci <2 2-4 >4	0 1 2 3
Portal inflammation arbitrary	absent mild moderate severe	0 1 2 3
Sinusoidal dilatation Grade	absent mild; involving ≤ 1/3 of the (centro-) lobular area moderate; involving 1/3-2/3 of the liver parenchyma severe; involving > 2/3 of the liver parenchyma	0 1 2 3
Parenchymal necrosis grade	absent affecting <25% of the parenchyma affecting 25%-50% of the parenchyma affecting 51-75% of the parenchyma affecting >75% of the parenchyma	0 1 2 3 4
Hepatocellular mitosis Per 8 HPF	not present <2 foci 2-4 5-10 >10	0 1 2 3 4
Councilman bodies Per 10x objective	not present <2 foci 2-4 5-10 >10	0 1 2 3 4

Table S2. Changes in miRNA expression in shApoB versus miApoB samples. Cellular small RNA data sets were annotated to miRBase (release 18, November 2011) and grouped based on the mature miRNA sequences and reads per million (rpm) were calculated. For each miRNA, proportion of the reads and the fold change between shApoB and miApoB (rpm) samples were calculated. If the proportion of the given miRNA from the shApoB sample was lower than proportion of the same miRNA in the miApoB (rpm) sample then this was represented by the negative value. Kal's test (Z-test) with Bonferroni correction was used to compare the proportions of miRNAs in the miApoB (rpm) versus shApoB sample. **p < 0.01

Name	miApoB (rpm)	shApoB (rpm)	Fold change	p value
mir-4521	2829	15	-188,60	0
mir-378c	5146	51	-100,90	<0,01**
mir-4326	462	13	-35,54	0
mir-720	688	52	-13,23	0
mir-3182	171	13	-13,15	0
mir-4454	68347	5281	-12,94	0
mir-4791	116	12	-9,67	0
mir-877	910	106	-8,58	<0,01**
mir-483	91	11	-8,27	0
mir-1280	2104	264	-7,97	0
mir-4286	15254	2127	-7,17	0
mir-4484	691	106	-6,52	<0,01**
mir-1260a	15492	2454	-6,31	0
mir-1260b	2977	494	-6,03	0
mir-4455	592	100	-5,92	<0,01**
mir-452	176	31	-5,68	<0,01**
mir-3127	51	10	-5,10	<0,01**
mir-1250	203	40	-5,08	0
mir-1299	176	35	-5,03	0
mir-4713	208	42	-4,95	0
mir-585	54	11	-4,91	<0,01**
mir-193a	302	63	-4,79	<0,01**
mir-551b	67	14	-4,79	<0,01**
mir-365a	83	18	-4,61	<0,01**
mir-1246	1872	406	-4,61	<0,01**
mir-2110	470	105	-4,48	<0,01**
mir-1268a	110	25	-4,40	0
mir-1247	78	18	-4,33	<0,01**
mir-3176	121	28	-4,32	0
mir-4473	82	19	-4,32	<0,01**
mir-1268b	116	27	-4,30	0
mir-4485	216	51	-4,24	0
mir-760	201	50	-4,02	<0,01**
mir-1227	44	11	-4,00	<0,01**
mir-210	11150	2794	-3,99	<0,01**
mir-1262	95	24	-3,96	<0,01**
mir-627	87	22	-3,95	<0,01**
mir-4470	135	36	-3,75	0

Table S2. continued

Name	miApoB (rpm)	shApoB (rpm)	Fold change	p value
mir-1261	52	14	-3,71	<0,01**
mir-3074	104	30	-3,47	<0,01**
mir-378i	1134	329	-3,45	<0,01**
mir-29c	339	100	-3,39	0
mir-504	81	24	-3,38	<0,01**
mir-3615	300	89	-3,37	0
mir-4746	168	50	-3,36	<0,01**
mir-491	341	103	-3,31	0
mir-505	33	10	-3,30	<0,01**
mir-193b	125	38	-3,29	<0,01**
mir-1290	178	56	-3,18	<0,01**
mir-1269b	1747	566	-3,09	<0,01**
mir-320c-1/2	188	61	-3,08	<0,01**
mir-1914	52	17	-3,06	<0,01**
mir-151b	326	108	-3,02	<0,01**
mir-146a	655	222	-2,95	<0,01**
mir-326	863	293	-2,95	<0,01**
mir-320a	58157	19821	-2,93	0
mir-4687	92	32	-2,88	<0,01**
mir-1249	180	63	-2,86	<0,01**
mir-573	37	13	-2,85	<0,01**
mir-3928	60	22	-2,73	<0,01**
mir-940	245	91	-2,69	<0,01**
mir-671	6969	2624	-2,66	0
mir-92b	69	26	-2,65	<0,01**
mir-3620	559	213	-2,62	<0,01**
mir-211	26	10	-2,60	<0,01**
mir-375	1962	762	-2,57	<0,01**
mir-328	783	311	-2,52	<0,01**
mir-1343	170	68	-2,50	<0,01**
mir-1180	4978	1995	-2,50	0
mir-4423	52	21	-2,48	<0,01**
mir-3136	95	39	-2,44	<0,01**
mir-148a	2964	1231	-2,41	<0,01**
mir-1269a	12	5	-2,40	<0,01**
mir-378d-1/2	1454	611	-2,38	<0,01**
mir-24-2	45	19	-2,37	<0,01**
mir-423	11893	5028	-2,37	0
mir-1255a	90	39	-2,31	<0,01**
mir-642b	46	20	-2,30	<0,01**
mir-501	376	164	-2,29	<0,01**
mir-2277	187	82	-2,28	<0,01**

Table S2. continued

Name	miApoB (rpm)	shApoB (rpm)	Fold change	p value
mir-942	410	182	-2,25	0
mir-133a-1/2	90	40	-2,25	<0,01**
mir-22	78	35	-2,23	<0,01**
mir-9-1/2/3	18571	8401	-2,21	<0,01**
mir-145	42	19	-2,21	<0,01**
mir-3943	24	11	-2,18	<0,01**
mir-574	392	180	-2,18	<0,01**
mir-1468	26	12	-2,17	<0,01**
mir-320d-1/2	93	43	-2,16	<0,01**
mir-339	18019	8358	-2,16	<0,01**
mir-3173	47	22	-2,14	<0,01**
mir-185	19368	9097	-2,13	<0,01**
let-7b	516	243	-2,12	<0,01**
mir-330	328	157	-2,09	<0,01**
let-7d	243	117	-2,08	<0,01**
mir-27a	165	80	-2,06	<0,01**
mir-28	1355	657	-2,06	<0,01**
mir-422a	101	49	-2,06	<0,01**
mir-296	358	175	-2,05	<0,01**
mir-744	3109	1523	-2,04	<0,01**
mir-1306	128	63	-2,03	<0,01**
mir-138-1/2	731	360	-2,03	<0,01**
mir-589	1938	974	-1,99	0
mir-378a	2067	1040	-1,99	<0,01**
mir-425	17334	8748	-1,98	0
mir-378f	537	275	-1,95	0
mir-151a	18918	9890	-1,91	0
mir-106b	18130	9486	-1,91	0
mir-542	107	56	-1,91	<0,01**
let-7c	3092	1628	-1,90	<0,01**
mir-629	5082	2682	-1,89	0
mir-708	3957	2093	-1,89	0
mir-320b-1/2	706	374	-1,89	0
mir-769	17874	9484	-1,88	0
mir-551a	139	74	-1,88	<0,01**
mir-345	7651	4077	-1,88	0
mir-29b-2	75	40	-1,88	<0,01**
mir-3944	298	160	-1,86	0
mir-1303	24	13	-1,85	<0,01**
mir-590	230	126	-1,83	<0,01**
mir-25	1151	635	-1,81	0
mir-5008	79	44	-1,80	<0,01**

Table S2. continued

Name	miApoB (rpm)	shApoB (rpm)	Fold change	p value
let-7i	2615	1458	-1,79	0
mir-152	4037	2334	-1,73	0
mir-1266	38	22	-1,73	<0,01**
mir-98	797	462	-1,73	0
mir-129-1/2	1111	649	-1,71	0
mir-27b	195	114	-1,71	<0,01**
mir-34a	16816	9849	-1,71	0
mir-628	46	27	-1,70	<0,01**
mir-548ab	100	59	-1,69	<0,01**
mir-1910	44	26	-1,69	<0,01**
mir-103a-2	1171	694	-1,69	0
mir-146b	11389	6806	-1,67	0
mir-4421	35	21	-1,67	<0,01**
mir-497	633	380	-1,67	0
mir-324	1118	682	-1,64	0
mir-194-1/2	7139	4362	-1,64	0
mir-139	36	22	-1,64	<0,01**
let-7g	19609	12000	-1,63	0
mir-7-1/2/3	123822	76717	-1,61	0
mir-1285-2	534	331	-1,61	<0,01**
mir-31	4700	2916	-1,61	<0,01**
mir-1307	1418	880	-1,61	0
mir-616	32	20	-1,60	<0,01**
mir-486	28634	17950	-1,60	0
mir-132	408	258	-1,58	0
mir-1286	17	11	-1,55	0,11
mir-93	49978	32504	-1,54	0
mir-101-2	53740	34952	-1,54	0
mir-217	39	26	-1,50	<0,01**
mir-3065	240	161	-1,49	<0,01**
mir-346	392	263	-1,49	<0,01**
mir-605	59	40	-1,48	<0,01**
mir-502	63	43	-1,47	<0,01**
mir-550a-1/2	328	225	-1,46	<0,01**
mir-103a-1	53323	37037	-1,44	0
mir-181c	1037	721	-1,44	<0,01**
mir-874	6180	4320	-1,43	<0,01**
mir-484	22583	15790	-1,43	0
mir-503	2035	1445	-1,41	0
mir-128-1/2	5142	3663	-1,40	0
mir-4677	53	38	-1,39	<0,01**
mir-188	236	170	-1,39	<0,01**

Table S2. continued

Name	miApoB (rpm)	shApoB (rpm)	Fold change	p value
mir-5585	54	39	-1,38	<0,01**
mir-548j	22	16	-1,38	0,13
mir-3130-1/2	59	43	-1,37	<0,01**
mir-17	208165	151899	-1,37	0
mir-204	177	130	-1,36	<0,01**
mir-218-1/2	32185	23741	-1,36	0
mir-186	79819	58927	-1,35	0
mir-548an	125	93	-1,34	<0,01**
mir-548aa-1/2	165	124	-1,33	<0,01**
mir-149	7087	5329	-1,33	0
mir-30b	15097	11479	-1,32	<0,01**
mir-1252	13	10	-1,30	0,29
mir-500a	822	638	-1,29	<0,01**
mir-181b-1/2	4027	3128	-1,29	<0,01**
mir-182	53787	42345	-1,27	0
mir-191	156325	123307	-1,27	0
mir-92a-1	694	548	-1,27	<0,01**
mir-1305	29	23	-1,26	0,14
let-7a-1/2/3	17874	14242	-1,26	0,00
mir-3909	257	205	-1,25	<0,01**
mir-576	259	207	-1,25	<0,01**
mir-1915	15	12	-1,25	0,30
mir-3662	30	24	-1,25	0,14
mir-4467	15	12	-1,25	0,30
mir-935	572	459	-1,25	<0,01**
mir-192	24042	19301	-1,25	0
mir-3140	66	53	-1,25	<0,01**
mir-548f-1/2/3/4	353	286	-1,23	<0,01**
mir-196a-1/2	16566	13441	-1,23	0
mir-130b	3712	3073	-1,21	0
mir-5699	65	54	-1,20	<0,01**
mir-3157	49	41	-1,20	0,09
mir-625	247	208	-1,19	<0,01**
mir-3611	38	32	-1,19	0,14
mir-891a	13	11	-1,18	0,40
mir-125b-1/2	12077	10462	-1,15	<0,01**
mir-598	637	557	-1,14	<0,01**
mir-618	714	629	-1,14	<0,01**
let-7e	2670	2361	-1,13	<0,01**
mir-362	13573	12026	-1,13	<0,01**
mir-1292	89	79	-1,13	0,05
mir-556	45	40	-1,13	0,17

Table S2. continued

Name	miApoB (rpm)	shApoB (rpm)	Fold change	p value
mir-219-1	292	263	-1,11	<0,01**
mir-18a	20829	18939	-1,10	<0,01**
mir-26b	6658	6060	-1,10	0
mir-1257	213	195	-1,09	<0,01**
mir-30a	54010	49483	-1,09	0
mir-489	13	12	-1,08	0,52
mir-580	65	60	-1,08	0,15
mir-652	169	157	-1,08	<0,01**
mir-651	136	127	-1,07	<0,01**
mir-33a	153	143	-1,07	<0,01**
mir-4792	291	273	-1,07	<0,01**
mir-499a	37	35	-1,06	0,32
mir-1301	1479	1409	-1,05	<0,01**
mir-19b-1	581	555	-1,05	<0,01**
mir-190b	24	23	-1,04	0,45
mir-34c	2365	2286	-1,03	<0,01**
mir-532	4923	4763	-1,03	<0,01**
mir-195	957	930	-1,03	<0,01**
mir-16-1/2	30082	29378	-1,02	0
mir-181d	1926	1883	-1,02	<0,01**
mir-2355	359	352	-1,02	<0,01**
mir-20b	52	51	-1,02	0,31
mir-1287	64	63	-1,02	0,27
mir-449a	70	69	-1,01	0,25
mir-99b	726091	721490	-1,01	0
mir-30d	57480	57397	-1,00	<0,01**
let-7f-1/2	11474	11467	-1,00	0
mir-23b	10	10	1,00	0,69
mir-133b	4	4	1,00	0,80
mir-3150a	18	18	1,00	0,59
mir-3174	12	12	1,00	0,66
mir-222	171	173	1,01	0,12
mir-190a	160	162	1,01	0,13
mir-1296	1177	1197	1,02	<0,01**
mir-641	434	444	1,02	<0,01**
mir-455	629	647	1,03	<0,01**
mir-338	148	153	1,03	0,20
mir-4786	29	30	1,03	0,58
mir-181a-1/2	11483	11939	1,04	<0,01**
mir-30e	128424	133609	1,04	0
mir-424	6753	7108	1,05	<0,01**
mir-140	1893	2035	1,08	<0,01**

Table S2. continued

Name	miApoB (rpm)	shApoB (rpm)	Fold change	p value
mir-454	128	138	1,08	0,40
mir-215	681	738	1,08	0,06
mir-1298	10	11	1,10	0,85
mir-26a-1/2	41047	46025	1,12	0
mir-21	101618	116255	1,14	0
mir-15a	4445	5096	1,15	<0,01**
mir-199a-1/2	13	15	1,15	0,92
mir-1278	13	15	1,15	0,92
mir-3613	3708	4324	1,17	0,25
mir-107	1545	1833	1,19	0,81
mir-15b	3097	3679	1,19	0,77
mir-196b	15868	18894	1,19	0,65
mir-5094	189	226	1,20	1,00
mir-3938	128	154	1,20	0,96
mir-450a-1/2	3134	3804	1,21	0,55
mir-125a	30443	36957	1,21	0,06
mir-548l	22	27	1,23	0,93
mir-548ag-1/2	79	97	1,23	0,86
mir-10b	1644920	2065460	1,26	0
mir-1-1/2	205	261	1,27	0,51
mir-4517	54	70	1,30	0,66
mir-548k	995	1293	1,30	0,05
mir-548t	13	17	1,31	0,81
mir-106a	1183	1572	1,33	<0,01**
mir-660	926	1236	1,33	<0,01**
mir-30c-1/2	24713	33382	1,35	0
mir-561	225	304	1,35	0,17
mir-421	1791	2438	1,36	<0,01**
mir-548e	566	787	1,39	<0,01**
mir-10a	3814906	5321388	1,39	0
mir-4652	15	21	1,40	0,64
mir-548h-1/2/3/4/5	144	204	1,42	0,12
mir-221	8370	12046	1,44	0
mir-212	358	526	1,47	<0,01**
mir-148b	146	215	1,47	0,05
mir-548n	61	90	1,48	0,21
mir-183	62636	92828	1,48	0
mir-2964a	16	24	1,50	0,48
mir-340	6854	10352	1,51	0
mir-548d-1/2	488	744	1,52	<0,01**
mir-331	118	182	1,54	<0,01**
mir-99a	155658	241891	1,55	0

Table S2. continued

Name	miApoB (rpm)	shApoB (rpm)	Fold change	p value
mir-1276	25	39	1,56	0,30
mir-450b	1194	1865	1,56	<0,01**
mir-2467	116	182	1,57	<0,01**
mir-548z	15	24	1,60	0,38
mir-100	471	764	1,62	<0,01**
mir-5683	35	57	1,63	0,15
mir-301a	149	249	1,67	<0,01**
mir-548w	100	173	1,73	<0,01**
mir-548o	76	133	1,75	<0,01**
mir-101-1	13	23	1,77	0,26
mir-582	495	885	1,79	<0,01**
mir-548aq	20	36	1,80	0,14
mir-941-1/2/3/4	3125	5688	1,82	<0,01**
mir-378g	221	416	1,88	<0,01**
mir-24-1	14	28	2,00	0,11
mir-199b	183	376	2,05	<0,01**
mir-548y	957	2069	2,16	0
mir-20a	62666	139055	2,22	<0,01**
mir-95	219	500	2,28	<0,01**
mir-548b	151	365	2,42	<0,01**
mir-1271	5483	13299	2,43	0
mir-579	22	54	2,45	0,00
mir-301b	271	703	2,59	<0,01**
mir-361	2307	5985	2,59	<0,01**
mir-1284	15	42	2,80	0,00
mir-96	27894	91513	3,28	<0,01**
mir-374b	448	1537	3,43	0,00
mir-126	115	399	3,47	<0,01**
mir-577	1403	5197	3,70	0
mir-624	59	234	3,97	0
mir-374a	486	1934	3,98	<0,01**
mir-548c/2/am	61	243	3,98	0
mir-32	139	626	4,50	0
mir-549	11	76	6,91	<0,01**
mir-548i-1/2/3/4	65	542	8,34	<0,01**
mir-18b	40	0	NA	<0,01**
mir-29a	39	0	NA	<0,01**
mir-124-1/2/3	53	0	NA	<0,01**
mir-135b	0	10	NA	<0,01**
mir-147b	11	0	NA	<0,01**
mir-153-1/2	0	16	NA	<0,01**
mir-184	12	0	NA	<0,01**

Table S2. continued

Name	miApoB (rpm)	shApoB (rpm)	Fold change	p value
mir-203	13	0	NA	<0,01**
mir-216a	0	11	NA	<0,01**
mir-216b	10	0	NA	<0,01**
mir-342	51	0	NA	<0,01**
mir-378b	43	0	NA	<0,01**
mir-449b	0	6	NA	<0,01**
mir-500b	55	0	NA	<0,01**
mir-548a-1/2	0	16	NA	<0,01**
mir-548a-3	10	0	NA	<0,01**
mir-548ad	0	5	NA	<0,01**
mir-548al	0	6	NA	<0,01**
mir-548au	0	16	NA	<0,01**
mir-548g/x/2	10	0	NA	<0,01**
mir-548u	0	10	NA	<0,01**
mir-550a-3	12	0	NA	<0,01**
mir-592	27	0	NA	<0,01**
mir-597	17	0	NA	<0,01**
mir-615	10	0	NA	<0,01**
mir-643	10	0	NA	<0,01**
mir-653	83	0	NA	<0,01**
mir-664	48	0	NA	<0,01**
mir-766	0	11	NA	<0,01**
mir-887	15	0	NA	<0,01**
mir-888	0	11	NA	<0,01**
mir-934	13	0	NA	<0,01**
mir-937	17	0	NA	<0,01**
mir-1255b-1/2	16	0	NA	<0,01**
mir-1272	10	0	NA	<0,01**
mir-1273c	38	0	NA	<0,01**
mir-1273d	10	0	NA	<0,01**
mir-1275	128	0	NA	0
mir-1285-1	12	0	NA	<0,01**
mir-1288	35	0	NA	<0,01**
mir-1294	0	12	NA	<0,01**
mir-1295a	34	0	NA	<0,01**
mir-1304	194	0	NA	0
mir-3131	20	0	NA	<0,01**
mir-3158-1/2	14	0	NA	<0,01**
mir-3178	88	0	NA	0
mir-3184	12	0	NA	<0,01**
mir-3196	16	0	NA	<0,01**
mir-3200	13	0	NA	<0,01**

Table S2. continued

Name	miApoB (rpm)	shApoB (rpm)	Fold change	p value
mir-3605	0	10	NA	<0,01**
mir-3661	14	0	NA	<0,01**
mir-3676	32	0	NA	<0,01**
mir-3691	11	0	NA	<0,01**
mir-3912	0	13	NA	<0,01**
mir-4461	39	0	NA	<0,01**
mir-4497	36	0	NA	<0,01**
mir-4523	25	0	NA	<0,01**
mir-4645	12	0	NA	<0,01**
mir-4664	13	0	NA	<0,01**
mir-4665	11	0	NA	<0,01**
mir-4742	11	0	NA	<0,01**
mir-4804	11	0	NA	<0,01**
mir-5100	88	0	NA	0
mir-5187	10	0	NA	<0,01**
mir-5579	0	22	NA	<0,01**
mir-5698	11	0	NA	<0,01**
mir-5701-1/2	61	0	NA	<0,01**

Table S3. Functional categorization of changes in shApoB injected animal. RPKM gene expression values were compared to shScr using Kal's test (Z-test) with Bonferroni correction. All genes that changed significantly in AAV-shApoB-injected animal ($p<0,05$) and were expressed higher than 0,1 (RPKM>0,1) were included in the analysis. Functional analysis of the significantly changing genes was done with the functional annotation tool DAVID (Database for Annotation, Visualization and Integrated Discovery v6.7; National Institute of Allergy and Infectious Diseases, NIH) that allows finding combination of co-ocurrent genes under study with respect to a reference list [49,50]. The annotations were done simultaneously with the reference to Gene Ontology databases (GOTERM_BP_FAT and GOTERM_MF_FAT, www.geneontology.org)) and to KEGG pathway database (KEGG_PATHWAY; www.genome.ad.jp/kegg/pathway.html). The redundancy in the gene list was manually analyzed and significant annotations were grouped in 8 categories and the percentage of genes in each category was calculated with reference to all genes that were annotated in DAVID analysis.

Genes found	Significant genes	Function annotations to GO, KEGG
	shApoB analysis	
	downregulated	
		Response to stimuli
11	KNG1, SERPINA3K, OAZ1, SERPINA1B, SERPINA6, SERPINA1A, SERPINF2, SERPINA1D, SERPINA1C, SERPINC1, SERPINA1E	BP:0034097~response to cytokine stimulus BP:0043434~response to peptide hormone stimulus MF:0004867~serine-type endopeptidase inhibitor activity BP:0009725~response to hormone stimulus KEGG: 04610:Complement and coagulation cascades
16	CYP2D9, CYP2C37, CYP2F2, CYP2C44, CYP2C67, CYP2C29, CYP4F14, CYP2E1, CYP1A2, CYB5, FTH1, TDO2, PGRMC1, CYP2A5, CAT, HPD	GO:0020037~heme binding GO:0046906~tetrapyrrole binding GO:0005506~iron ion binding GO:0009055~electron carrier activity
8	SERPINA3K, SERPINA1B, SERPINA1A, ALB, APOE, SERPINA1D, SERPINA1C, SERPINA1E	BP:0009719~response to endogenous stimulus BP:0010033~response to organic substance
8	SERPINA3K, SERPINA1B, SERPINA1A, SERPINA1D, SERPINA1C, ALDOB, SERPINA1E, AGXT	MF:0004866~endopeptidase inhibitor activity MF:0030414~peptidase inhibitor activity MF:0004857~enzyme inhibitor activity
		Lipid metabolism and transport
8	APOA2, APOB, APOE, APOC4, APOC3, APOC1, APOC2	MF:0006869~lipid transport MF:0010876~lipid localization MF:0042157~lipoprotein metabolic process

upregulated		
		Lipid metabolism and transport
2	RDH9, LPL, APOA4	MF:0042157~lipoprotein metabolic process BP:0008610~lipid biosynthetic process GO:0008202~steroid metabolic process
		Drug metabolism
12	CYP2C70, GSTM1, GSTA1, GSTA2, GSTM2, UGT1A9, GSTM3, GSTM4, CYP3A11, UGT2B1, UGT2B5, EPHX1	KEGG: 00982:Drug metabolism
8	CYP2C70, CYP2A12, UGT1A9, CYP4A12A, CYP3A11, UGT2B1, UGT2B5, CYP2A4	mmu00982:Drug metabolism mmu00830:Retinol metabolism GO:0070330~aromatase activity mmu00983:Drug metabolism
		Inflammation
9	C8A, SERPINA3N, SAA2, SERPINA1B, HC, C3, SERPINA1A, SAA1, AHSG	BP:0002526~acute inflammatory response BP:0006954~inflammatory response BP:0006953~acute-phase response
7	SERPINA3N, PZP, SERPINA7, HC, C3, ITIH4, AHSG	MF:0004866~endopeptidase inhibitor activity MF:0030414~peptidase inhibitor activity MF:0004857~enzyme inhibitor activity MF:0004867~serine-type endopeptidase inhibitor activity
		Cell growth and death
7	C8A, GPX1, LYZ2, KRT18, HC, KRT8, CLU	BP:0019835~cytolysis BP:0008219~cell death BP:0016265~death
		Response to stimuli
8	EGR1, FOS, APOA2, GCK, HPX, GPX4, JUN, NR4A1	BP:0010033~response to organic substance BP:0010604~positive regulation of macromolecule metabolic process BP:0051789~response to protein stimulus BP:0051173~positive regulation of nitrogen compound metabolic process BP:0010033~response to organic substance
		MAPK singalling pathway
5	FOS, DUSP1, JUN, NR4A1, DUSP6	KEGG:04010 MAPK signaling pathway

Table S4. Functional categorization of changes in miApoB injected animals. RPKM gene expression values were compared to miScr using Kal's test (Z-test) with Bonferroni correction. All genes that changed significantly in AAV-miApoB-injected animal ($p<0,05$) and were expressed higher than 0,1 (RPKM>0,1) were included in the analysis. Functional analysis of the significantly changing genes was done with the functional annotation tool DAVID (Database for Annotation, Visualization and Integrated Discovery v6.7; National Institute of Allergy and Infectious Diseases, NIH) that allows finding combination of co-ocurrent genes under study with respect to a reference list [49,50]. The annotations were done simultaneously with the reference to Gene Ontology databases (GOTERM_BP_FAT and GOTERM_MF_FAT, www.geneontology.org)) and to KEGG pathway database (KEGG_PATHWAY; www.genome.ad.jp/kegg/pathway.html). The redundancy in the gene list was manually analyzed and significant annotations were grouped in 8 categories and the percentage of genes in each category was calculated with reference to all genes that were annotated in DAVID analysis.

Genes found	Significant genes	Function annotations to GO, KEGG
		miApoB analysis
		downregulated
		Drug metabolism
22	GSTA1, GSTA2, GSTA4, CYP2C54, CYP2C44, CYP2C67, UGT2B1, CYP1A2, GSTM1, CYP2A12, GSTM2, GSTM3, UGT1A9, GSTM4, UGT2B34, FMO1, ADH4, CYP2A5, UGT2B5, CYP2D26, MGST1, CYP2A4	KEGG:00982:Drug metabolism KEGG:00980:Metabolism of xenobiotics by cytochrome P450 KEGG: 00480:Glutathione metabolism
10	GSTM1, GSTA1, GSTA2, GSTM2, GSTM3, GSTM4, GSTA4, GM3776, MGST1	MF:0004364~glutathione transferase activity MF:0016765~transferase activity, transferring alkyl or aryl (other than methyl) groups
36	SC5D, CYP2C44, CYP2F2, HSD3B7, CYP2C67, HSD3B5, UGDH, FTH1, AKR1C14, RDH9, CYP2A12, TDO2, CYP4A12A, FMO1, ADH4, HMOX1, BC089597, HSD17B6, IDH1, DMGDH, CAT, HPD, SCD1, CYP2C54, FADS1, FADS2, CYP1A2, CYP7B1, CYP27A1, H6PD, HSD11B1, CYP2A5, AOX3, CYP2D26, HPGD, CYP2A4	BP:0055114~oxidation reduction BP:0008202~steroid metabolic process MF:0016229~steroid dehydrogenase activity
7	G6PC, UGT1A9, UGT2B34, UGT2B1, UGT2B5, UGDH, UGP2	KEGG:00500:Starch and sucrose metabolism KEGG:00140:Steroid hormone biosynthesis KEGG:00053:Ascorbate and aldarate metabolism KEGG:00983:Drug metabolism KEGG:00150:Androgen and estrogen metabolism KEGG:00232:Caffeine metabolism

		Lipid metabolism and transport
6	APOB, APOA4, LDLR, PCSK9, APOM, APOBEC2	MF:0006869~lipid transport MF:0010876~lipid localization
11	ABCG8, NPC1, G6PC, APOB, FECH, LDLR, MLXIPL, PCSK9, SCARB1, NR5A2, MTP	GO:0055092~sterol homeostasis GO:0055088~lipid homeostasis
12	RDH9, GC, CYP7B1, G6PC, SC5D, SERPINA6, HSD3B7, HSD3B5, INSIG1, HSD11B1, HSD17B6, CAT	BP:0008610~lipid biosynthetic process GO:0008202~steroid metabolic process
10	G6PC, APOB, INSIG2, ANG, SERINC1, INSIG1, PCSK9, CAT, FABP5, MTP	GO:0046486~glycerolipid metabolic process GO:0006641~triglyceride metabolic process
7	SC5D, ELOVL3, FADS1, ELOVL2, FASN, FADS2, SC4MOL	GO:0006633~fatty acid biosynthetic process
		Ion binding and transport
26	SC5D, FTL1, CYP2F2, CYP2C44, CYP2C67, TRF, FTH1, CYP2A12, TDO2, CYP4A12A, HMOX1, PGRMC1, CAT, HPD, SCD1, CYP2C54, FADS1, FADS2, CYP1A2, CYP7B1, CYP27A1, CYP2A5, AOX3, CYP2D26, SLC40A1, CYP2A4	MF:0005506~iron ion binding MF:0020037~heme binding MF:0046906~tetrapyrrole binding MF:0016712~oxidoreductase activity MF:0070330~aromatase activity MF:0009055~electron carrier activity
		Response to sitmuli
18	KNG1, PZP, MUG1, C3, SERPING1, SERPINA3K, PZP, SERPINA3N, SERPINA3M, SERPINA1B, SERPINA6, SERPINA1D, SERPINA1C, ITIH4, SERPINC1, ITIH2, SERPIND1, ITIH3	BP:0009611~response to wounding BP:0034097~response to cytokine stimulus BP:0050817~coagulation BP:0007596~blood coagulation BP:0007599~hemostasis BP:0042060~wound healing BP:0009725~response to hormone stimulus BP:0050878~regulation of body fluid levels BP:0009719~response to endogenous stimulus
8	SCD1, CYP4A12A, ACSL1, CYP27A1, FADS2, FABP5, CPT1A, PCK1	mmu03320:PPAR signaling pathway

STable S4. continued

Genes found	Significant genes	Function annotations to GO, KEGG
		miApoB analysis
		upregulated
		Oxidoreductase activity and processes
33	ATP5D, ATP5E, NDUFB6, NDUFB7, NDUFB9, COX7C, COX5A, COX5B, UQCRQ, ATP5G3, NDUFB2, NDUFS5, UQCR10, UQCR11, COX6B1, ATP5L, ATP5O, ATP5H, NDUFS2, ATP5K, ATP5J, NDUFA4, NDUFA5, NDUFA2, ATP5J2, NDUFA3, NDUFB10, COX4I1, NDUFC1, COX6C, UQCRH, COX6A1, UQCRB	KEGG:00190:Oxidative phosphorylation BP:0006091~generation of precursor metabolites and energy BP:0022900~electron transport chain BP:0055114~oxidation reduction
		Lipid metabolism and transport
7	CYP4A10, ACAA2, ADH1, CYP4A14, ACAA1A, ACAA1B, ALDH3A2	KEGG:00071:Fatty acid metabolism KEGG:03320:PPAR signaling pathway MF:0003988~acetyl-CoA C-acyltransferase activity GO:0006641~triglyceride metabolic process GO:0046486~glycerolipid metabolic process
11	APOA2, APOE, APOC4, APOC3, APOC1, LPL GPX1, PIGYL, PEMIT, SLC27A5	MF:0006869~lipid transport MF:0010876~lipid localization MF:0042157~lipoprotein metabolic process
18	CYB5R3, HSD17B11, EBP, PCTP, AMACR, APOC1, FDPS, AKR1C20, APOA2, APOA1, AKR1C6, APOE, APOF, SULT1A1, APOC3, PON1, LIPC, SLC27A5	GO:0008202~steroid metabolic process GO:0008203~cholesterol metabolic process
		Nucleobase, nucleoside and nucleotide biosynthetic processes
20	ATP5D, ATP5E, COX7C, COX4I1, COX5A, COX5B, UQCRQ, ATP5G3, COX6C, UQCR10, UQCR11, UQCRH, COX6B1, COX6A1, ATP5L, ATP5O, ATP5H, ATP5K, ATP5J, UQCRB	BP:0006754~ATP biosynthetic process BP:0046034~ATP metabolic process BP:0034654~nucleobase, nucleoside, nucleotide and nucleic acid biosynthetic process

Table S5. Comparison of lipid-related gene expression profiles in AAV-shApoB, AAV-miApoB and siApoB injected animals based on our NGS data and siApoB Taqman data from Tep *et al.* (48). For each entry the fold change between sample and respective negative control were calculated. If expression of a given gene in the sample was lower than expression in the negative control the fold change had a negative value.

Gene	AAV-shApoB	AAV-miApoB	siApoB
Aacs	-1,11	-1,29	-2,60
Acaca	-2,50	-1,55	-2,08
Acacb	-2,51	1,07	-4,81
Acat2	1,04	1,49	-2,14
Acly	-2,34	1,06	-1,75
Acsf2	-1,40	1,13	2,00
Acsl1	-1,62	-1,29	-1,26
Acsl3	-1,25	1,35	-1,85
Acsl4	-2,63	1,96	-2,02
Acsl5	-1,64	-1,13	-2,24
Acss2	-1,49	-1,18	-3,49
ActB	1,49	1,69	1,00
Adi1	1,24	1,20	-1,78
Agpat1	1,52	1,20	-1,27
Agpat2	-1,12	1,11	-1,67
Agpat3	-1,36	1,30	-1,67
Agpat4	1,04	1,26	10,00
Agpat5	2,12	1,63	-1,05
Agpat6	1,42	1,17	-1,25
Agpat9	1,90	1,67	-1,11
Angptl4	1,94	-1,22	-4,76
ApoA1	1,16	-1,13	-1,93
ApoB	-11,83	-3,12	-8,27
ApoC3	1,26	-1,63	-1,00
ApoE	1,50	-1,23	-1,08
Baat	-1,21	1,30	-1,39
Cds1	-1,93	1,08	-1,86
Chpt1	1,18	-1,13	-1,45
Cyb5r3	1,31	-1,49	-1,91
Cyp27a1	-1,54	-1,06	-1,77
Cyp39a1	-1,79	1,79	-3,00
Cyp46a1	1,46	-1,17	-1,27
Cyp7a1	1,27	1,76	1,19
Cyp7b1	-2,20	1,17	-2,47
Cyp8b1	1,06	-1,36	-1,57
Dgat1	1,34	1,17	-5,55
Dgat2	-1,12	1,07	-1,90
Dhcr24	-1,34	1,29	-1,80
Dhcr7	-1,39	1,46	-1,25
Elovl1	1,74	-1,06	-3,55

Table S5. continued

Gene	AAV-shApoB	AAV-miApoB	siApoB
Elovl2	1,14	1,77	-3,80
Elovl3	-2,03	1,51	1,79
Elovl4	-1,79	1,14	-5,22
Elovl5	-1,52	1,24	-3,19
Elovl6	-1,42	1,31	-3,49
Fads1	-1,83	1,12	-3,72
Fads2	-2,08	2,07	-2,00
Fads3	1,09	1,32	-2,45
Fasn	-2,63	1,32	-1,62
Fdft1	1,21	1,20	-2,87
Fdps	1,54	1,08	-1,09
Gpat	1,88	1,24	-1,92
Gpr65	1,01	3,02	-1,11
Haao	1,07	-1,41	-1,47
Hmgcr	-1,28	1,82	-2,06
Hmgcs1	-1,44	1,59	-9,09
Hsd17b6	-5,37	-1,30	-1,96
Hsd3b7	-1,38	1,14	-2,52
Idi1	-1,56	1,19	-1,19
Ldlr	-1,75	1,23	-1,42
Lpcat4 (Agpat7)	1,38	1,44	-4,54
Lrp8	ND	ND	4,17
Lycat (Agpat8)	ND	ND	-1,72
Mogat1	ND	ND	1,96
Mogat2	ND	ND	1,19
Mtp	-1,85	1,21	-1,59
Mvd	1,20	1,66	-1,81
Mvk	-1,59	1,09	1,96
Pcsk9	-2,69	1,02	-1,59
Pcyt2	1,10	-1,30	-1,63
Pmvk	1,13	1,34	-3,21
Ppap2a	-1,47	1,31	-50,53
Ppap2b	-1,03	1,38	-1,07
Ppap2c	-1,49	1,03	-1,13
Ppara	-1,32	1,06	-1,37
Ppard	-1,58	2,19	-2,16
Pparg	2,16	1,47	-2,00
Ppia	1,01	-1,21	-1,09
Scap	-1,01	-1,04	-1,04
Scarb1	-1,79	1,42	-1,14
Scd1	-3,14	-1,63	-4,92
Scd2	-1,25	2,24	2,08

Supplementary Table 5. continued

Gene	AAV-shApoB	AAV-miApoB	siApoB
Sgpl1	-1,99	1,10	-1,09
Sgpp1	1,09	1,46	-1,02
Slc27a5	1,03	1,20	-1,75
Soat1	1,49	3,80	-1,96
Soat2	-1,47	-1,46	-1,81
Splc1	ND	ND	-1,35
Srebf2	-1,59	1,35	-1,41
Stard3	1,39	1,19	-1,20
Tm7sf2	1,62	-1,04	-2,55
Vldlr	ND	ND	-1,04
Xpnep3	-2,19	1,83	1,35

Table S6. Antibodies used in the study

Antibody	Host	Code	Dilution	Incubation time/temp
CK-18[1]	Rabbit	1924-1	1:200	60 min, RT
Ki67 (Clone SP6)[2]	Rabbit	RM-9106-S0	1:2000	60 min, RT
CD31[3]	Rabbit	LS-B4737-250	1:50	Overnight, 4°C
Cleaved Caspase-3[4]	Rabbit	9661L	1:200	60 min, RT
AP Polymer anti-Rabbit[5]	-	MON-APP201	undiluted	30 min, RT
HRP Plymer anti-Rabbit[5]	-	MON-APP202	undiluted	30 min ,RT

RT- room temperature
[1] Epitomics,Inc, Burlingame, CA
[2] Thermo Fisher Scientific/Labvision, Fremont, CA
[3] LifeSpan Biosciences Inc., Seattle, WA
[4] Cell Signaling Technology Inc., Danvers, MA
[5] MONOSAN, Uden, The Netherlands

Reference list

1. Fire, A, Xu, S, Montgomery, MK, Kostas, SA, Driver, SE and Mello, CC (1998). Potent and specific genetic interference by double-stranded RNA in Caenorhabditis elegans. *Nature*; **391:** 806-811.
2. Paddison, PJ, Caudy, AA, Bernstein, E, Hannon, GJ and Conklin, DS (2002). Short hairpin RNAs (shRNAs) induce sequence-specific silencing in mammalian cells. *Genes Dev*; **16:** 948-958.
3. Soutschek, J, Akinc, A, Bramlage, B, Charisse, K, Constien, R, Donoghue, M, et al. (2004). Therapeutic silencing of an endogenous gene by systemic administration of modified siRNAs. *Nature*; **432:** 173-178.
4. Boudreau, RL, Martins, I and Davidson, BL (2009). Artificial microRNAs as siRNA shuttles: improved safety as compared to shRNAs in vitro and in vivo. *Mol Ther*; **17:** 169-175.
5. Grimm, D (2009). Small silencing RNAs: State-of-the-art. *Adv Drug Deliv Rev*; **61:** 672-703.
6. Zamore, PD, Tuschl, T, Sharp, PA and Bartel, DP (2000). RNAi: double-stranded RNA directs the ATP-dependent cleavage of mRNA at 21 to 23 nucleotide intervals. *Cell*; **101:** 25-33.
7. Ahn, M, Witting, SR, Ruiz, R, Saxena, R and Morral, N (2011). Constitutive expression of shRNA in vivo triggers build up of mature hairpin molecules. *Hum Gene Ther*; **22:** 1483-1497.
8. Borel, F, van Logtenstein R., Koornneef, A, Maczuga, P, Ritsema, T, Petry, H, et al. (2011). In vivo knock-down of multidrug resistance transporters ABCC1 and ABCC2 by AAV-delivered shRNAs and by artificial miRNAs. *J RNAi Gene Silencing*; **7:** 434-442.
9. Bridge, AJ, Pebernard, S, Ducraux, A, Nicoulaz, AL and Iggo, R (2003). Induction of an interferon response by RNAi vectors in mammalian cells. *Nat Genet*; **34:** 263-264.
10. Grimm, D, Streetz, KL, Jopling, CL, Storm, TA, Pandey, K, Davis, CR, et al. (2006). Fatality in mice due to oversaturation of cellular microRNA/short hairpin RNA pathways. *Nature*; **441:** 537-541.
11. Sledz, CA, Holko, M, de Veer, MJ, Silverman, RH and Williams, BR (2003). Activation of the interferon system by short-interfering RNAs. *Nat Cell Biol*; **5:** 834-839.
12. Jackson, AL, Bartz, SR, Schelter, J, Kobayashi, SV, Burchard, J, Mao, M, et al. (2003). Expression profiling reveals off-target gene regulation by RNAi. *Nat Biotechnol*; **21:** 635-637.
13. McBride, JL, Boudreau, RL, Harper, SQ, Staber, PD, Monteys, AM, Martins, I, et al. (2008). Artificial miRNAs mitigate shRNA-mediated toxicity in the brain: Implications for the therapeutic development of RNAi. *Proc Natl Acad Sci U S A*; **105:** 5868-5873.
14. Giering, JC, Grimm, D, Storm, TA and Kay, MA (2008). Expression of shRNA from a tissue-specific pol II promoter is an effective and safe RNAi therapeutic. *Mol Ther*; **16:** 1630-1636.
15. Maczuga, P, Koornneef, A, Borel, F, Petry, H, van Deventer, S, Ritsema, T, et al. (2012). Optimization and comparison of knockdown efficacy between polymerase II expressed shRNA and artificial miRNA targeting luciferase and Apolipoprotein B100. *BMC Biotechnol*; **12:** 42.
16. Judge, AD, Sood, V, Shaw, JR, Fang, D, McClintock, K and MacLachlan, I (2005). Sequence-dependent stimulation of the mammalian innate immune response by synthetic siRNA. *Nat Biotech*; **23:** 457-462.
17. Kariko, K, Bhuyan, P, Capodici, J, Ni, H, Lubinski, J, Friedman, H, et al. (2004). Exogenous siRNA mediates sequence-independent gene suppression by signaling through toll-like receptor 3. *Cells Tissues Organs*; **177:** 132-138.
18. Kleinman, ME, Yamada, K, Takeda, A, Chandrasekaran, V, Nozaki, M, Baffi, JZ, et al. (2008). Sequence- and target-independent angiogenesis suppression by siRNA via TLR3. *Nature*; **452:** 591-597.
19. Witting, SR, Brown, M, Saxena, R, Nabinger, S and Morral, N (2008). Helper-dependent adenovirus-mediated short hairpin RNA expression in the liver activates the interferon response. *J Biol Chem*; **283:** 2120-2128.
20. Kenworthy, R, Lambert, D, Yang, F, Wang, N, Chen, Z, Zhu, H, et al. (2009). Short-hairpin RNAs delivered by lentiviral vector transduction trigger RIG-I-mediated IFN activation. *Nucleic Acids Res*; **37:** 6587-6599.
21. Jackson, AL and Linsley, PS (2010). Recognizing and avoiding siRNA off-target effects for target identification and therapeutic application. *Nat Rev Drug Discov*; **9:** 57-67.
22. Boudreau, RL, Spengler, RM and Davidson, BL (2011). Rational design of therapeutic siRNAs: minimizing off-targeting potential to improve the safety of RNAi therapy for Huntington's disease. *Mol Ther*; **19:** 2169-2177.

23. Caffrey, DR, Zhao, J, Song, Z, Schaffer, ME, Haney, SA, Subramanian, RR, et al. (2011). siRNA off-target effects can be reduced at concentrations that match their individual potency. *PLoS ONE*; **6:** e21503.
24. Maczuga, P, Lubelski, J, van Logtenstein, R, Borel, F, Blits, B, Fakkert, E, et al. (2013). Embedding siRNA sequences targeting Apolipoprotein B100 in shRNA and miRNA scaffolds results in differential processing and in vivo efficacy. *Mol Ther*; **21:** 217-227.
25. Young, SG (1990). Recent progress in understanding apolipoprotein B. *Circulation*; **82:** 1574-1594.
26. Rozema, DB, Lewis, DL, Wakefield, DH, Wong, SC, Klein, JJ, Roesch, PL, et al. (2007). Dynamic PolyConjugates for targeted in vivo delivery of siRNA to hepatocytes. *Proc Natl Acad Sci U S A*; **104:** 12982-12987.
27. Tarugi, P, Averna, M, Di, LE, Cefalu, AB, Noto, D, Magnolo, L, et al. (2007). Molecular diagnosis of hypobetalipoproteinemia: an ENID review. *Atherosclerosis*; **195:** e19-e27.
28. Visser, ME, Akdim, F, Tribble, DL, Nederveen, AJ, Kwoh, TJ, Kastelein, JJ, et al. (2010). Effect of apolipoprotein-B synthesis inhibition on liver triglyceride content in patients with familial hypercholesterolemia. *J Lipid Res*; **51:** 1057-1062.
29. Rawlings, ND, Tolle, DP and Barrett, AJ (2004). Evolutionary families of peptidase inhibitors. *Biochem J*; **378:** 705-716.
30. Silverman, GA, Bird, PI, Carrell, RW, Church, FC, Coughlin, PB, Gettins, PG, et al. (2001). The serpins are an expanding superfamily of structurally similar but functionally diverse proteins. Evolution, mechanism of inhibition, novel functions, and a revised nomenclature. *J Biol Chem*; **276:** 33293-33296.
31. Irving, JA, Pike, RN, Lesk, AM and Whisstock, JC (2000). Phylogeny of the serpin superfamily: implications of patterns of amino acid conservation for structure and function. *Genome Res*; **10:** 1845-1864.
32. Martin, LJ and Tremblay, JJ (2009). The nuclear receptors NUR77 and SF1 play additive roles with c-JUN through distinct elements on the mouse Star promoter. *J Mol Endocrinol*; **42:** 119-129.
33. Shao, Q, Shen, LH, Hu, LH, Pu, J, Qi, MY, Li, WQ, et al. (2010). Nuclear receptor Nur77 suppresses inflammatory response dependent on COX-2 in macrophages induced by oxLDL. *J Mol Cell Cardiol*; **49:** 304-311.
34. Bermudez, O, Pagès, G and Gimond, C (2010). The dual-specificity MAP kinase phosphatases: critical roles in development and cancer. *Am J Physiol Cell Physiol*; **299:** C189-C202.
35. Suhy, DA, Kao, SC, Mao, T, Whiteley, L, Denise, H, Souberbielle, B, et al. (2012). Safe, long-term hepatic expression of anti-HCV shRNA in a nonhuman primate model. *Mol Ther*; **20:** 1737-1749.
36. Tadin-Strapps, M, Peterson, LB, Cumiskey, AM, Rosa, RL, Mendoza, VH, Castro-Perez, J, et al. (2011). siRNA induced liver ApoB knockdown lowers serum LDL-cholesterol in a mouse model with human-like serum lipids. *J Lipid Res*; **52:** 1084-1097
37. Zimmermann, TS, Lee, AC, Akinc, A, Bramlage, B, Bumcrot, D, Fedoruk, MN, et al. (2006). RNAi-mediated gene silencing in non-human primates. *Nature*; **441:** 111-114.
38. Crooke, RM, Graham, MJ, Lemonidis, KM, Whipple, CP, Koo, S and Perera, RJ (2005). An apolipoprotein B antisense oligonucleotide lowers LDL cholesterol in hyperlipidemic mice without causing hepatic steatosis. *J Lipid Res*; **46**: 872-884.
39. Visser, ME, Akdim, F, Tribble, DL, Nederveen, AJ, Kwoh, TJ, Kastelein, JJ, et al. (2010). Effect of apolipoprotein-B synthesis inhibition on liver triglyceride content in patients with familial hypercholesterolemia. *J Lipid Res*; **51:** 1057-1062.
40. Savary, S, Trompier, D, Andreoletti, P, Le, BF, Demarquoy, J and Lizard, G (2012). Fatty acids-induced lipotoxicity and inflammation. *Curr Drug Metab*; **13**:1358-1370
41. Penaud-Budloo, M, Le Guiner, C, Nowrouzi, A, Toromanoff, A, Ch+¬rel, Y, Chenuaud, P, et al. (2008). Adeno-Associated Virus Vector Genomes Persist as Episomal Chromatin in Primate Muscle. *J Virol*; **82:** 7875-7885.
42. Castanotto, D, Sakurai, K, Lingeman, R, Li, H, Shively, L, Aagaard, L, et al. (2007). Combinatorial delivery of small interfering RNAs reduces RNAi efficacy by selective incorporation into RISC. *Nucleic Acids Res*; **35:** 5154-5164.
43. Keck, K, Volper, EM, Spengler, RM, Long, DD, Chan, CY, Ding, Y, et al. (2009). Rational design leads to more potent RNA interference against hepatitis B virus: factors effecting silencing efficiency. *Mol Ther*; **17:** 538-547.
44. Flood, C, Gustafsson, M, Pitas, RE, Arnaboldi, L, Walzem, RL and Boren, J (2004). Molecular mechanism for changes in proteoglycan binding on compositional changes of the core and the surface of low-density lipoprotein-containing human apolipoprotein B100. *Arterioscler Thromb Vasc Biol*; **24:** 564-570.

45. Olivecrona, G and Olivecrona, T (2010). Triglyceride lipases and atherosclerosis. *Curr Opin Lipidol*; **21:** 409-415.
46. Okuyama, S, Marusawa, H, Matsumoto, T, Ueda, Y, Matsumoto, Y, Endo, Y, et al. (2012). Excessive activity of apolipoprotein B mRNA editing enzyme catalytic polypeptide 2 (APOBEC2) contributes to liver and lung tumorigenesis. *Int J Cancer*; **130:** 1294-1301.
47. Mikl, MC, Watt, IN, Lu, M, Reik, W, Davies, SL, Neuberger, MS, et al. (2005). Mice deficient in APOBEC2 and APOBEC3. *Mol Cell Biol*; **25:** 7270-7277.
48. Tep, S, Mihaila, R, Freeman, A, Pickering, V, Huyhn, F, Tadin-Strapps, M, et al. (2012). Rescue of Mtp siRNA-induced hepatic steatosis by DGAT2 siRNA silencing. *J Lipid Res*; **53:** 859-867.
49. Koornneef, A, Maczuga, P, van Logtenstein, R, Borel, F, Blits, B, Ritsema, T, et al. (2011). Apolipoprotein B knockdown by AAV-delivered shRNA lowers plasma cholesterol in mice. *Mol Ther*; **19:** 731-740.
50. van der Loos, CM (2008). Multiple immunoenzyme staining: methods and visualizations for the observation with spectral imaging. *J Histochem Cytochem*; **56:** 313-328.
51. Chen, C, Ridzon, DA, Broomer, AJ, Zhou, Z, Lee, DH, Nguyen, JT, et al. (2005). Real-time quantification of microRNAs by stem-loop RT-PCR. *Nucleic Acids Res*; **33:** e179.
52. Livak, KJ and Schmittgen, TD (2001). Analysis of relative gene expression data using real-time quantitative PCR and the 2-[delta][delta] CT method. *Methods*; **25:** 402-408.
53. Mortazavi, A, Williams, BA, McCue, K, Schaeffer, L and Wold, B (2008). Mapping and quantifying mammalian transcriptomes by RNA-Seq. *Nat Methods*; **5:** 621-628.
54. Edgar, R, Domrachev, M and Lash, AE (2002). Gene Expression Omnibus: NCBI gene expression and hybridization array data repository. *Nucleic Acids Res*; **30:** 207-210.
55. Szklarczyk, D, Franceschini, A, Kuhn, M, Simonovic, M, Roth, A, Minguez, P, et al. (2011). The STRING database in 2011: functional interaction networks of proteins, globally integrated and scored. *Nucleic Acids Res*; **39:** D561-D568.
56. Huang, dW, Sherman, BT and Lempicki, RA (2009). Systematic and integrative analysis of large gene lists using DAVID bioinformatics resources. *Nat Protoc*; **4:** 44-57.
57. Huang, dW, Sherman, BT and Lempicki, RA (2009). Bioinformatics enrichment tools: paths toward the comprehensive functional analysis of large gene lists. *Nucleic Acids Res*; **37:** 1-13.